Journal of Radioanalytical and Nuclear Chemistry
https://doi.org/10.1007/s10967-025-10494-4

The potential of gold nanoparticles in prostate-specific membrane antigen-targeted radioligand therapy for future treatment of metastatic castration-resistant prostate cancer

Sumandi Juliyanto[1,2] · Rien Ritawidya[1] · Ahsanal Fikri[1] · Amal Rezka Putra[1] · Herlan Setiawan[1] · Maskur[1] · Muammar Fawwaz[3] · Yoki Yulizar[2]

Received: 11 June 2025 / Accepted: 16 October 2025

Abstract
Prostate-specific membrane antigen-targeted radioligand therapy is a potent new treatment that improves survival and quality of life in metastatic castration-resistant prostate cancer patients. However, these require high radiation doses and frequent delivery; hence, innovative strategies to develop future therapeutic agents are needed. Gold nanoparticles' ability to deliver a large payload of radionuclides, favorable bioavailability, modifiable surfaces, and ability to induce hyperthermia could potentially enhance efficacy when combined with targeted radioligand therapeutic agents. Recent advances in targeted gold nanoparticles and their radiolabeling with potential radioligands, radiobiology, and photothermal effects to facilitate combination therapies are discussed in this review.

✉ Yoki Yulizar
yokiy@sci.ui.ac.id

Sumandi Juliyanto
sumandi.juliyanto@brin.go.id

[1] Research Center for Radioisotopes, Radiopharmaceuticals, and Biodosimetry Technology, National Research and Innovation Agency (BRIN), Kawasan Puspiptek, Setu, Tangerang Selatan 15314, Indonesia

[2] Department of Chemistry, Faculty of Mathematics and Natural Sciences, Universitas Indonesia, UI-Campus, Beji, Depok, West Java 16424, Indonesia

[3] Laboratory of Pharmaceutical Chemistry, Faculty of Pharmacy, Universitas Muslim Indonesia, Jl. Urip Sumihardjo Km.5, Kampus II UMI, Makassar, Indonesia

Published online: 04 November 2025

Graphical abstract

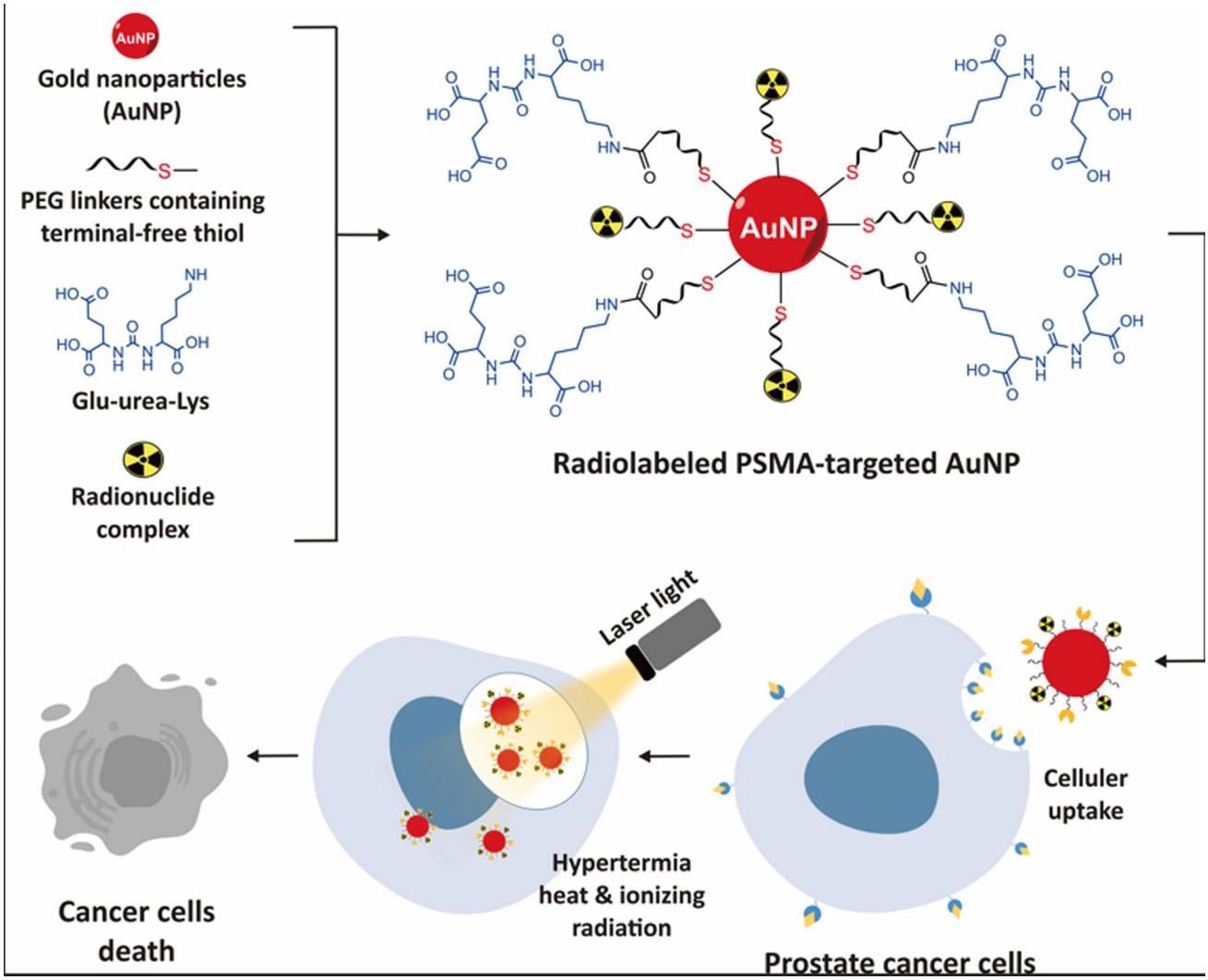

Keywords Gold nanoparticle · Metastatic castration-resistant prostate cancer · Prostate-specific membrane antigen · Targeted radioligand therapy

Introduction

Based on the oncology database GLOBOCAN 2022, prostate cancer is the second most prevalent cancer, and it remains a major concern in terms of public health [1, 2]. The statistics from Cancer Statistics 2025 further confirm that prostate cancer was the most prevalent diagnosed cancer among men in the United States in 2025, accounting for 30% of new cases [3]. Effective and appropriate management of prostate cancer has become a critical approach to reducing the number of deaths. Additionally, the accurate and sensitive method for staging the disease also plays a crucial role in the selection of the therapeutic approach [4, 5]. To determine the stage of prostate cancer suffered by patients, diagnostic modalities have been developed based on prostate-specific antigen (PSA) levels, the Gleason score derived from prostate biopsy, and advanced imaging modalities such as magnetic resonance imaging (MRI), positron emission tomography (PET), PET/MRI, and PET/computed tomography (PET/CT) for patients with high-risk characteristics [5–7].

Prostate cancer therapy options are classified as low-risk, intermediate-risk, high-risk, and end-stage prostate cancer [5]. Localized low-risk patients can be treated with radical prostatectomy and brachytherapy, while localized intermediate-risk and high-risk patients can be treated

with external-beam radiation therapy (EBRT) or in conjunction with androgen deprivation therapy (ADT) [5, 7, 8]. In cases of high-risk metastatic disease, it can be treated with second-generation ADT (abiraterone or enzalutamide), and chemotherapy (docetaxel or cabazitaxel) can be used when ADT is ineffective [1]. In end-stage prostate cancer, the patient's testosterone levels remain low despite receiving abiraterone or enzalutamide and chemotherapy using docetaxel or cabazitaxel, become resistant, and PSA begins to rise again, which is known as metastatic castration-resistant prostate cancer (mCRPC) [1, 7]. Most cases of prostate cancer progress to this stage, and mCRPC is the second most common cause of cancer-related death in adult males [5, 9]. mCRPC presents a significant social and economic challenge, necessitating effective therapeutic alternatives.

In recent years, targeted radioligand therapy (TRLT) has been widely developed and is a promising new therapeutic approach for mCRPC [5, 9, 10]. TRLT's primary system consists of a radionuclide complex/particle linked to a vector molecule (ligand) that selectively binds to tumor-specific receptors [9, 11]. Immediately after the ligand complex's internalization, the radionuclide particle is released intracellularly, resulting in DNA damage and cell death. Radionuclides utilized in TRLT for mCRPC comprise alpha (α) and beta (β^-) emitters [11]. This is due to radionuclides emitting α or β^- particles being more effective for treating solid tumors, while those emitting Äuger electrons are utilized for targeting individual cancer cells or small clusters of cancer cells due to their short-range biological effectiveness (the path length of most Auger electrons is < 1 μm) [12–14]. TRLT for mCRPC treatment has the advantage of naturally accumulating or being designed to target and deliver a specific amount of cytotoxic radiation to prostate cancer cells without affecting the surrounding normal tissue. This allows for the treatment of multiple bone and extraskeletal metastases at the same time [10]. However, research is ongoing to find ways to maximize the advantages of TRLT while remaining safe and effective for each mCRPC patient.

Prostate-specific membrane antigen (PSMA) is a type II transmembrane glycoprotein with 750 amino acids, also known as folate hydrolase I or glutamate carboxypeptidase II [15, 16]. PSMA is expressed at all stages of prostate cancer, with levels 100–1000-fold higher (correlated with cancer grade) compared to the kidneys, small intestine, duodenal mucosa, salivary gland, liver, spleen, neuroendocrine cells in the colonic crypts, and brain [6, 15–17]. PSMA exhibits high tissue specificity for prostate cancer, making it a crucial target for prostate cancer therapy and diagnosis, especially for mCRPC [7].

Initial PSMA-TRLT was the capromab pendetide labeled with yttrium-90 (^{90}Y), but a phase II study discovered 75% of cases of hematologic toxicity when treated with [^{90}Y] Y-capromab without lowering serum prostate-specific antigen levels [16, 18]. To enhance targeting, a humanized monoclonal antibody, J591, was developed that targets the extracellular domain of PSMA and was labeled with lutetium-177 (^{177}Lu) for therapeutic use [19, 20]. However, long blood circulation time, lowered vascular permeability, and poor penetration of large solid tumors by antibodies may result in heterogeneous tumor doses and a lower likelihood of tumor control [16, 21, 22]. To address this issue, numerous studies of PSMA-TRLT were conducted with small-molecule PSMA inhibitors serving as radioligands and demonstrating higher penetration in large solid tumors and lower hematotoxicity than monoclonal antibodies [15, 16]. The utilization of small-molecule PSMA inhibitors may provide numerous benefits over larger entities in the production of TRLT, including diminished immunogenicity and lower scale-up expenses. These inhibitors have favorable pharmacokinetic properties, high affinity and specificity for PSMA, and rapid uptake in PSMA-expressing cancer cells [22, 23].

TRLT-based small-molecule PSMA inhibitors (sPSMAi-TRLT) have been shown to have a significant impact on mCRPC treatment [23, 24]. In this regard, PSMA-617 and PSMA I&T (Fig. 1) are prominent examples of small-molecule PSMA inhibitors [25–27]. PSMA-617 and PSMA I&T are the most utilized ligands for the development of radiolabeled pharmaceuticals targeting PSMA in mCRPC [9, 28]. They are constructed of three parts: a binding motif or pharmacophore (glutamate-urea-lysine [Glu-urea-Lys]), a radiolabeled moiety (chelator) for complexing radionuclide, and a linker that connects these two entities [22, 26, 29]. The Glu-urea-Lys binding motif, as shown in Fig. 1, derived from PSMA's natural substrate, N-acetyl-L-aspartyl-L-glutamate (NAAG), is incorporated into small molecule inhibitors to increase their binding affinity and specificity for PSMA [22]. The high level of binding affinity of the Glu-urea-Lys motif to PSMA depends on interactions of the glutamic acid residue with the S1-binding pocket as well as the binding of the urea functionality to the Zn^{2+} active center [23, 30]. Furthermore, lipophilic interactions of the Glu-urea-Lys motif with the hydrophobic S1-accessory pocket and the arene-binding site further enhance the PSMA binding affinity and selectivity [24]. Meanwhile, the Glu-urea-Lys motif's lysine residue serves as a binding site for a linker [22].

The radiopharmaceutical sPSMAi-TRLT has been used in clinical settings and has received approval from the European Medicines Agency (EMA) and the US Food and Drug Administration (FDA) for the treatment of mCRPC adult patients who have been treated with ADT and docetaxel-based or taxane-based chemotherapy [5, 7, 28, 31]. However, the use of sPSMAi-TRLT has limitations that lead to adverse side effects for patients, such as the need for high radiation doses and frequent administration [9, 26]. To overcome these limitations, it is necessary to develop a delivery

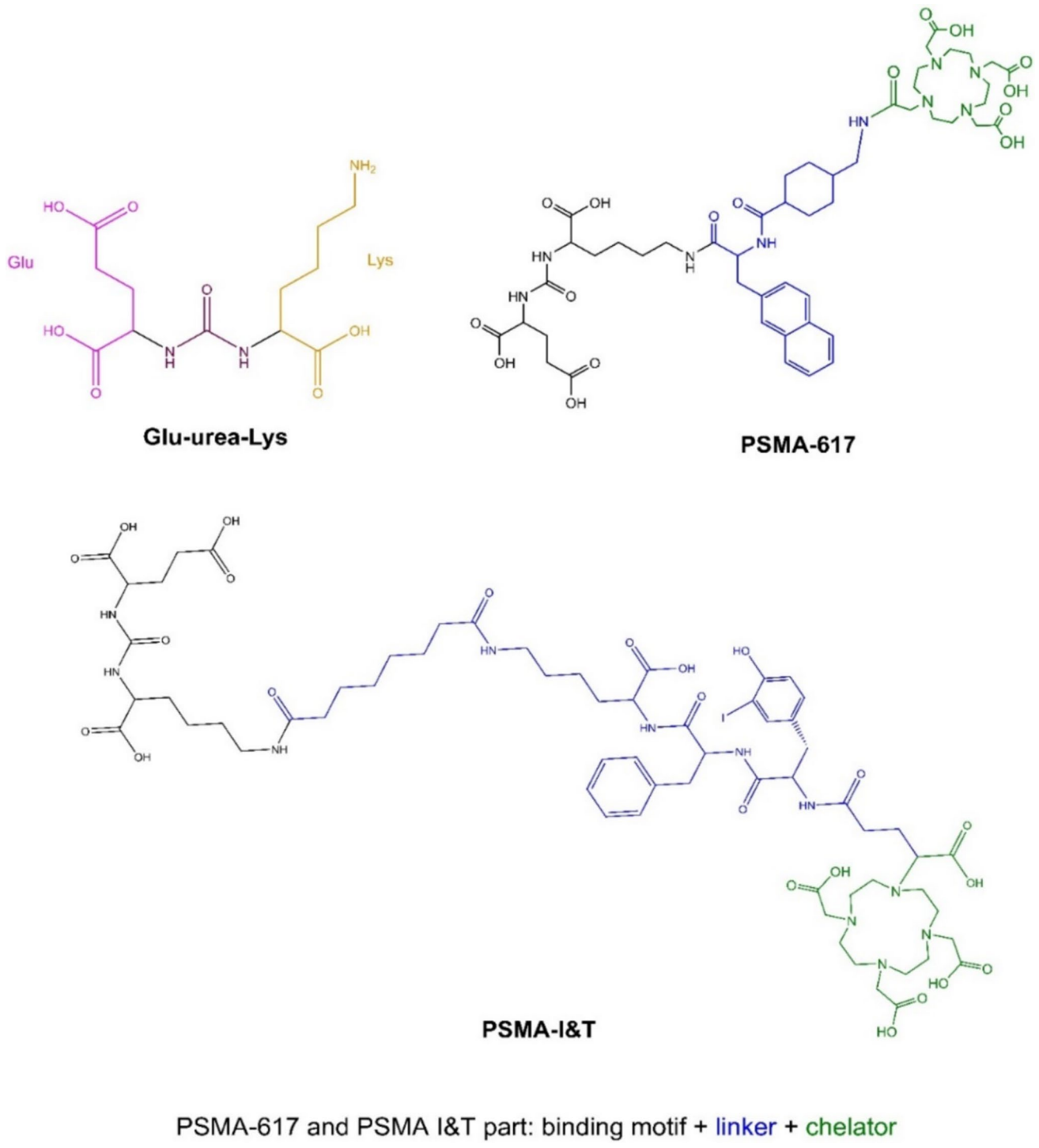

Fig. 1 Chemical structures of Glu-urea-Lys, PSMA-617, and PSMA I&T

system that can potentially increase the effective dose of sPSMAi-TRLT while also combining it with other therapeutic strategies that provide a synergistic effect, increasing the therapeutic efficacy.

Gold nanoparticles (AuNPs) are a versatile material that can be processed into a variety of shapes and sizes. Taking advantage of their unique physicochemical properties, AuNPs are frequently utilized as contrast agents, radiosensitizers in cancer diagnosis and therapy, and photothermal agents [32]. The use of AuNPs as radiosensitizers provides a significant advantage in their application in TRLT for theranostic agents. Radiosensitizers are compounds or

particles that increase the effective dose of radiotherapy in cancer cells [33]. The high atomic number of AuNPs (Z = 79) enhances radionuclide dose deposition, increasing the efficacy of internal radionuclide therapies [33, 34]. In addition to their ability to increase radionuclide dose deposition, AuNPs can have biological effects on cancer cells. AuNPs can catalyze the production of reactive oxygen species (ROS) and interfere with antioxidant defense systems. As a result, oxidative stress can lead to mitochondrial dysfunction, DNA damage, autophagy, apoptosis, and arrest of the G2/M cell cycle, the most radiosensitive phase [35]. This AuNP's biological effects potentially cause cancer cells to have a reduced ability to respond adequately to ionizing radiation, making them more sensitive to TRLT.

The ability of AuNPs to deliver a variety of medically relevant radionuclides expands their application in TRLT. The surface of AuNPs has been modified with chelators containing radionuclides and targeted to cell surface receptors using various targeting moieties [36]. There are three main advantages of using AuNPs as therapeutic radionuclide carrier agents: obtaining much higher payloads of radioactivity as compared to a conventional radiopharmaceutical agent, can effectively extravasate through the interstices between endothelial cells of the leaky and immature blood vessels into the tumor but the retention in the tumor tissue is enhanced, and the large surface area-to-volume ratio of AuNPs provides the biofunctionalization of the AuNPs surface with multiple cancer-targeting molecules through the high affinity for thiols and amino groups [35, 37, 38]. Therefore, the surface of AuNPs can be easily modified to bind targeting molecules such as small-molecule PSMA inhibitors [39, 40]. Furthermore, AuNPs have been demonstrated to have low or no cytotoxicity due to their relatively inert characteristics when compared to other types of nanostructures, making them ideal for therapeutic use [41].

AuNPs, which are both biocompatible and photostable, are excellent photothermal agents that have been extensively studied for their ability to generate hot electrons via localized surface plasmon resonance (LSPR) [42]. LSPR is caused by the restricted oscillation of free electron clouds in their lattice when irradiated with resonant frequency light [37, 43]. Furthermore, surface plasmon waves resonate with electromagnetic waves from the light source, leading to plasma decay into excited primary electrons via Landau damping, resulting in inelastic scattering of electrons. The secondary electrons formed are captured on the AuNPs surface, resulting in non-radiative damping relaxation of the energetic electrons, which causes excessive heat in the particles and the surrounding microenvironment [43, 44]. On a picosecond time scale, electron relaxation on the AuNPs surface converts into heat [45]. Utilizing a light frequency at or near the surface plasmon resonance absorption of AuNPs generates a hyperthermic environment efficiently, which holds significant potential for the selective ablation of tumor tissue in photothermal therapy (PTT) applications [37].

The localized hyperthermia heat from PTT application via AuNPs can potentially enhance the efficacy of TRLT for cancer treatment [46]. PTT has advantages as a cancer treatment modality, including the fact that it is non-invasive and has the potential to reduce adverse side effects on normal cells while increasing toxicity to tumor cells [47]. Furthermore, PTT has other advantages, such as the ability to induce the formation of cytotoxic species solely through the control of light at specific wavelengths and a low prevalence of resistance phenomena [43].

This review aims to provide a brief and specific overview of AuNPs' potential for improved sPSMAi-RLT efficacy, which is particularly useful for addressing mCRPC in the future. We will investigate the conjugation mechanism and surface modification of AuNPs that could potentially be used to produce PSMA-targeted AuNPs that are conveniently radiolabeled with radionuclides. Furthermore, the concept of combination therapy based on the photothermal properties of AuNPs, which can simultaneously target multiple cancer proliferation pathways, shows great promise for improving treatment outcomes and dealing with cancer cell resistance from TRLT. This comprehensive strategy is essential to control the dynamic process of prostate cancer and ultimately improve patient survival rates. By overcoming the barriers of TRLT, we aim to contribute to the advancement of future prostate cancer treatment, especially in the mCRPC stage, providing hope and better outcomes for patients impacted by the disease.

Current research studies on sPSMAi-RLT for mCRPC treatment

The development of sPSMAi-RLT agents is inextricably linked to the advancement of high-affinity small-molecule PSMA inhibitor-based imaging agents. Early generations of sPSMAi-RLT agents were created simply by replacing imaging agents' radionuclides with therapeutics. Later, extensive structure–activity relationship studies were carried out to address the safety and efficacy issues raised by initial patient data [22]. Small-molecule PSMA inhibitors have been labeled with beta- (β^-) and alpha (α)-emitting radionuclides. Therefore, this section will divide the description of sPSMAi-RLT agent studies into two sections based on the two types of ionizing radiation.

α-particle-emitting radionuclide-based sPSMAi-RLT

Alpha (α) particle-emitting radionuclides have special characteristics that make them extremely effective at killing cancer cells, which is high linear energy transfer (LET)

[22]. The amount of energy deposited per unit length by ionizing radiation is referred to as LET, and high LET in α-emitting radionuclides indicates that α particles are more damaging than other types of ionizing radiation at the same dose [21]. This high LET is due to the particle's physical properties, notably a heavy helium nucleus and a short path length of up to 100 µm in water-equivalent tissue and 40 µm in bone (with LET values ranging from 50 to 230 keV/µm), which lead to localized cell killing [21, 22]. These characteristics may cause more direct DNA damage with no spillover to nearby cells, reducing side effects on normal tissue and causing more double-strand breaks that are more difficult to repair, making α-emitting radionuclides more effective in hypoxic tissues [21, 48]. However, α-emission is a high-energy process associated with the recoil of the daughter radionuclide. This recoil may lead to radiolysis in the radiopharmaceutical, resulting in the release of the daughter radionuclide. If the recoil occurs inside the cell, it can contribute to overall cytotoxicity by remaining in the tumor; conversely, if the recoil happens outside the cell, the circulating daughter radionuclide could harm healthy organs such as the kidney [21, 49].

The rapid tumor uptake with small-molecule PSMA inhibitors has been proposed as one way to address the recoil effect and was employed to mitigate its negative effects [21, 50]. Rapid uptake permits daughter radionuclides to be emitted and retained intratumorally without entering the circulation. Few α-emitting radionuclides have been evaluated for efficacy and safety in treating mCRPC by complexing with small-molecule PSMA inhibitors, as shown in Table 1. In mCRPC clinical trials, only bismuth-213 (^{213}Bi)- and actinium-225 (^{225}Ac)-based sPSMAi-RLT have been studied. [10, 21, 22].

Sathekge and colleagues observed the inaugural human therapeutic efficacy of [^{213}Bi]Bi-PSMA-617 in a patient with progressive mCRPC undergoing standard treatment. The total activity of 592 MBq administered across two cycles produced a favorable biochemical response, evidenced by a PSA reduction exceeding 80% [51]. However, clinical trials of [^{213}Bi]Bi-PSMA-617 stopped after Kratochwil and colleagues discovered that it had a lower therapeutic index and a higher radiation dose to the kidney than [^{225}Ac]Ac-PSMA-617. This happens because [^{213}Bi]Bi-PSMA-617 experiences more perfusion-dependent off-target radiation, and the biological half-life of PSMA-617 in dose-limiting organs is longer than the physical half-life of ^{213}Bi, making this radionuclide a second choice for α-particle-emitting radionuclide-based PSMA-RLT [52].

Among the developed α-particle-emitting TRLTs based on the glu-urea-lysine targeting motif, [^{225}Ac]Ac-PSMA-617 has been evaluated in multiple clinical retrospective studies [21]. Kratochwil et al. conducted the first human study of [^{225}Ac]Ac-PSMA-617, evaluating two mCRPC patients with challenging clinical situations treated with 100 kBq/kg at bimonthly intervals as salvage therapy after [^{68}Ga]Ga-PSMA-11 PET/CT validated the presence of a PSMA-positive tumor phenotype. As a result, both patients' PSA levels declined below measurable levels, but both had xerostomia as dose-limiting toxicity [53]. Kratochwil et al. also investigated the efficacy of [^{225}Ac]Ac-PSMA-617 in 40 mCRPC patients who received extensive pretreatment with chemotherapy, radiotherapy, and androgen deprivation therapy (abiraterone (85%) and enzalutamide (60%)). The investigation found that 63% of patients had a PSA decline of more than 50%, with a median overall survival of more than 12 months [54]. Ballal et al. studied the long-term survival outcomes of salvage [^{225}Ac]Ac-PSMA-617 therapy in 63 mCRPC patients who had received a total of 204 cycles. The findings revealed that 91% of patients had a decline in PSA, with patients having a PSA decline of more than 50% and a median overall survival of 15 months [55].

The efficacy of α-emitting radionuclide-based sPSMAi-RLT in prostate cancer therapy, such as [^{225}Ac]Ac-PSMA-617, could potentially be greater than that of β$^-$-emitting radionuclide-labeled small-molecule PSMA inhibitors, such as [^{177}Lu]Lu-PSMA-617, but it has a higher toxicity profile, and comparative data confirming its claimed efficacy are lacking [1, 64]. Given the physiological expression of PSMA in the kidneys and the primary renal excretion of [^{225}Ac]Ac-PSMA-617, there is apprehension regarding potential radiation toxicity to the kidneys. It has been reported that after [^{225}Ac]Ac-PSMA-617 therapy, kidney function deteriorated in a patient with one functional kidney, and chronic kidney disease was discovered in two patients with mCRPC [65, 66]. This is mostly because the radioactive daughter products of ^{225}Ac, but not the [^{225}Ac]Ac-PSMA-617, can accumulate in tubular cells and irradiate the kidney, causing kidney damage [66].

In a study investigated by Feuerecker et al. with [^{225}Ac]Ac-PSMA-617, all patients experienced some degree of dry mouth, and six patients (23%) requested that treatment be discontinued due to this side effect [67]. In another study, Sathekge et al. applied [^{225}Ac]Ac-PSMA-617 and found that 81% (43/53) of patients had grade 1 or 2 xerostomia [68]. These can happen due to alpha radiation, which can increase the occurrence of xerostomia in the ^{225}Ac ligand [1]. In particular, 100 kBq/kg was determined to be the maximum tolerable activity of [^{225}Ac]Ac-PSMA-617, with xerostomia serving as the dose-limiting toxicity [21]. This undoubtedly presents challenges in the future advancement of α-particle-emitting radionuclide-based sPSMAi-RLT.

β$^-$-particle-emitting radionuclide-based sPSMAi-RLT

B$^-$-emitting radionuclides are ionizing particles that increase reactive oxygen species (ROS)-mediated DNA damage

Table 1 α-emitting radionuclides appropriate for complexation with small-molecule PSMA inhibitors for mCRPC treatment

Radionuclide	Half-life	$E_{\alpha(max)}$ (MeV)	Total α energy emitted per decay (MeV)	LET (keV/µm)	Range in tissue (µm)	Radioligand complex	Advantage	Drawbacks	Reference
^{149}Tb	4.1 h	3.97	0.7	140	25–28	[^{149}Tb]Tb-PSMA-617	Preclinical studies showed that the [^{149}Tb]Tb-PSMA-617 group encountered slower tumor growth than the control group, which received normal saline injections	• The radiation dose to the kidneys is more than ten times that of [^{177}Lu]Lu-PSMA-617 • The high recoil energy causes radiolysis of the radiopharmaceutical, which leads to the spread of these long-lived bone-seeking daughter radionuclides ^{149}Eu ($t_{1/2}$ = 93 d) and ^{145}Sm ($t_{1/2}$ = 340 d), increasing the bone marrow and whole-body radiation dose	[10, 21, 22, 56, 57]
^{212}Pb	10.6 h	6.05	7.9	61–230	40–100	[^{212}Pb]Pb-NG001	In athymic nude mice containing C4-2 xenografts, injecting only 0.32 MBq of [^{212}Pb]Pb-NG001 resulted in increased survival compared to the control group, with a therapeutic index of > 2.0	The recoil energy is high enough to lead 36% of the daughter radionuclide, ^{212}Bi, to dissociate from the radioligand, delivering a higher radiation dose to the kidneys	[10, 21, 22, 58, 59]
^{211}At	7.2 h	6.79	6.9	71–230	55–80	[^{211}At]At-DCAtBzL	[^{211}At]At-DCAtBzL was found to effectively treat primary tumors and micrometastases	In a one-year dose-escalation study, [^{211}At]At-DCAtBzL accumulated in renal proximal microtubules due to overexpression of PSMA in rodent proximal tubes, resulting in severe nephropathy even with a single dose of 37 kBq of [^{211}At]At-DCAtBzL and chronic radiotoxicity in the kidneys	[21, 22, 60]

Table 1 (continued)

Radionuclide	Half-life	$E_{\alpha(max)}$ (MeV)	Total α energy emitted per decay (MeV)	LET (keV/μm)	Range in tissue (μm)	Radioligand complex	Advantage	Drawbacks	Reference
^{223}Ra	11.4 d	5.64	26.8	71–230	45–70	[^{223}Ra]Ra -macropa-Glu-urea-Glu	The [^{223}Ra]Ra-macropa complex revealed high long-term stability in vitro under physiological conditions and in vivo in murine models	The targeted form of the [^{223}Ra]Ra-macropa complex is inaccessible due to the absence of a biologically stable chelator complex	[21, 22, 61]
^{213}Bi	45.6 min	8.32	8.5	65–230	40–100	[^{213}Bi]Bi-L1, [^{213}Bi]Bi-PSMA-617	• [^{213}Bi]Bi-L1 showed specific cell uptake and cell death in prostate cancer cells • A cumulative activity of 592 MBq of [^{213}Bi]Bi-PSMA-617 administered over two cycles in a patient with progressive mCRPC resulted in a good biochemical response, with a prostate-specific antigen (PSA) reduction of more than 80%	• Because of its short half-life, ^{213}Bi is unsuitable for routine therapeutic applications due to logistical challenges • [^{213}Bi]Bi-PSMA-617 had a lower therapeutic index and enhanced radiation dose to the kidneys	[21, 22, 52, 62]
^{225}Ac	10.0 d	6.83	27.9	61–230	47–85	[^{225}Ac]Ac-PSMA-617, [^{225}Ac]Ac- PSMA-I&T	• The efficacy of [^{225}Ac]Ac-PSMA-617 was evaluated in 40 mCRPC patients and revealed a PSA decline of more than 50% in 63% of patients, with a median overall survival of more than 12 months • The first clinical data using [^{225}Ac]Ac-PSMA-I&T revealed highly comparable biochemical responses to [^{225}Ac]Ac-PSMA-617	Xerostomia was identified as a frequent adverse reaction, prompting 10–25% of patients to discontinue treatment with [^{225}Ac]Ac-PSMA-617 and [^{225}Ac]Ac-PSMA-I&T	[10, 21, 22, 55, 63]

(70%) and direct DNA damage (30%) [69, 70]. They have a low LET and may induce single-strand DNA breaks over a longer range, making them ideal for larger tumors [31, 71]. β^--emitting radionuclides interfere with cell cycle and signaling, resulting in tumor regression with minimal off-target effects on surrounding tissues. They inhibit cancer cell proliferation by causing apoptosis and cell cycle arrest [70]. Low doses of β^--emitting radionuclides enhance toxicity and induce apoptosis in cancer cells, while high doses cause cell cycle arrest in the G0/G1 phase [70, 72]. The list of radionuclides that have desirable properties that enable them to be complexed with small-molecule PSMA inhibitors is summarized in Table 2.

In terms of therapeutic application, only yttrium-90 (^{90}Y), iodine-131 (^{131}I), and lutetium-177 (^{177}Lu) are FDA-approved among the β^--radiating radionuclides [70]. Previously, ^{90}Y and ^{131}I were used in preclinical studies because they were readily available. The main issue with ^{90}Y is its long-range and higher β^--energy radiation in comparison with ^{177}Lu, which could raise the risk of off-target radiotoxicity in kidneys and other normal tissues [22, 73]. Likewise, one limitation of ^{131}I-based therapeutics is their inherent metabolic instability in vivo, which leads to accumulation in tissues such as the thyroid, making ^{131}I-based radiopharmaceutical therapy dose-limited [22].

^{177}Lu is the most frequently utilized radionuclide in preclinical and clinical therapy studies due to its relatively long half-life and cost-effectiveness, and due to its widespread availability [22, 28, 74]. Therapy with ^{177}Lu-labeled small-molecule PSMA inhibitors is an option for patients with advanced mCRPC [5]. The macrocyclic chelator 1,4,7,10-tetraazacyclododecane-1,4,7,10-tetraacetic acid (DOTA) is frequently employed for the development of small-molecule PSMA inhibitors (PSMA-617 and PSMA I&T), especially for the complexation of trivalent (+ 3) ions like [^{177}Lu]Lu^{3+}, which resulted in a thermodynamically and kinetically stable complex binding [23, 75].

DOTA chelator and [^{177}Lu]Lu^{3+} ion form a nine-coordinated complex with a stability constant of approximately 25.4 [76, 77]. The [^{177}Lu]Lu-DOTA complex has a higher stability constant value than the [^{177}Lu]Lu^{3+} ion complex with the chelators diethylenetriaminepentaacetic acid (DTPA), ethylenediaminetetraacetic acid (EDTA), nitrilotriacetic acid (NTA), 1,4,7,10-tetraazacyclododecane-1,4,7-triacetic acid (DO3A), and 1,4,7-triazacyclononane-1,4,7-triacetic acid (NOTA), with values of 12.5, 19.8, 22.4, 23.0, and 15.3, respectively [76]. This suggests that [^{177}Lu]Lu-DOTA is the most stable complex and is unable to easily dissociate and release the [^{177}Lu]Lu^{3+} ion under physiological conditions. Our research group developed the radiolabeling of antibodies, including Trastuzumab and Nimotuzumab, utilizing the [^{177}Lu]Lu-DOTA complex, demonstrating favorable in vitro and in vivo stability [78, 79]. DOTA's four arms, which each contain a carboxylate functional group, form a stable binding with [^{177}Lu]Lu^{3+} [77]. Chemically, the DOTA can form a strong complex with [^{177}Lu]Lu^{3+} in the center following one hydration; the basal plane is occupied by four macrocycle amine nitrogens, the capped plane by four carboxylic residue oxygens, and the capping position by a water molecule, resulting in close square antiprism geometry coordination, as shown in Fig. 2 [75, 76].

The radiolabeling method of small-molecule PSMA inhibitors with the radiometal cation [^{177}Lu]Lu^{3+} was a simple complexation reaction. In the instance of DOTA chelators with slow reaction kinetics for metal complexation, heating the labeling mixture is frequently required to ensure quantitative binding of the radiometal and thus replicate quantitative radiochemical yields [24]. This is in line with the PSMA-617 (0.5–5 nmol) radiolabeling method with [^{177}Lu]Lu^{3+} (20 MBq) reported by Benesova et al., which employed a reaction temperature of 95°C for 20 min [26]. Chakraborty et al. reported radiolabeling of [^{177}Lu]Lu^{3+} with PSMA-617 by adding 20 µL of [^{177}Lu]$LuCl_3$ (185 MBq, 19.1 nmol) solution to 20 µL of PSMA-617 (conc. 1 mg/mL) and 0.1 M ammonium acetate buffer of pH 5, followed by reaction for 30 min at 90 °C [29]. Furthermore, C.A. Wieczorek Villas Boas et al. performed a complexation reaction with PSMA-617 (10 µg) diluted in 200 µL of 0.52 M ascorbate buffer, pH 4.7, and 740 MBq of [^{177}Lu]$LuCl_3$ (23 µL) for 30 min at 90 °C [80].

The radiolabeling reaction of [^{177}Lu]Lu^{3+} with PSMA-617 requires acetate or ascorbate buffer due to the acidic

Table 2 β^--emitting radionuclides appropriate for radiolabeling on small-molecule PSMA inhibitors for targeted prostate cancer therapy

Radionuclide	Half-life	$E_{\beta(max)}$ (keV)	Range in tissue max (mm)	Radiopharmaceutical (radiation activity)	References
^{90}Y	2.67 d	2284	11.3	[^{90}Y]Y-PSMA-617 (2.8–3.7 GBq)	[22, 81]
^{131}I	8.02 d	606	2.1	[^{131}I]I-DCIBzL (3.7–8.4 GBq)	[12, 22, 82]
^{177}Lu	6.73 d	497	1.8	[^{177}Lu]Lu-PSMA-617 (2.0–8.0 GBq), [^{177}Lu]Lu-PSMA-I&T (3.3–7.8 GBq)	[22, 24, 31]
^{67}Cu	2.58 d	575	2.1	[^{67}Cu]Cu-RPS-085 (2.0–8.0 GBq)	[22, 83]
^{161} Tb	6.90 d	589	2.2	[^{161}Tb]Tb-PSMA-617 (5.5 GBq)	[22, 84, 85]

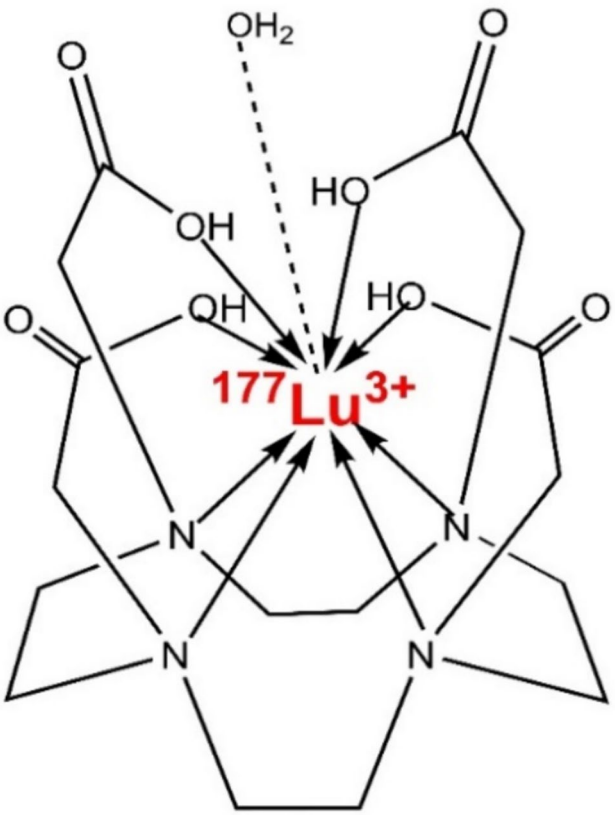

Fig. 2 Representative chemical structure of the [^{177}Lu]Lu-DOTA complex

properties of the radiometal solution ([^{177}Lu]$LuCl_3$) and the pH dependence of the reaction [24]. After the reaction was completed, the reaction mixture was allowed to cool to room temperature before the radiolabeled conjugate was purified from uncomplexed [^{177}Lu]Lu^{3+} with a C_{18} Sep-Pak cartridge [24, 29].

The radiochemical purity was determined using thin-layer chromatography on a silica gel 60 plate (TLC-SG) as the stationary phase with 0.1 M citrate buffer pH 5.0 as the mobile phase. The TLC-SG strips were evaluated using a radio TLC scanner; within this system, the [^{177}Lu]Lu-PSMA-617 revealed Rf 0.1–0.2, while the free lutetium-177 Rf was 0.9–1.0. Radiochemical purity can also be determined using the radio-HPLC method, which uses a C-18 column eluted at a flow rate of 0.4 mL/min by (A) water 0.1% TFA and (B) acetonitrile in the following gradient mode: 0–2 min 17% B; 2.01–5.99 min 30% B; 6–20 min 17% B. In this system, free lutetium-177 and [^{177}Lu]Lu-PSMA-617 were eluted in around 4.3 and 12.17 min, respectively [80].

Radiopharmaceutical therapy targeting PSMA with β^--particle emitting radionuclides, especially small–molecule PSMA inhibitors, [^{177}Lu]Lu-PSMA-617, is a life-prolonging treatment option for patients with mCRPC [22, 86]. It has demonstrated low toxicity profiles compared to the standard of care and has received regulatory approval [22, 86, 87]. Initial clinical investigations with [^{177}Lu]Lu-PSMA-617 showed that PSA levels decreased in both a multicenter retrospective cohort and a single-arm phase 2 trial [88, 89]. Sartor et al. discovered that [^{177}Lu]Lu-PSMA-617 significantly increased survival, delayed symptomatic skeletal events, prolonged the time to worsening health-related quality of life and pain, and delayed biochemical progression when compared to patients who received standard care only [86]. According to the international randomized open-label phase III VISION clinical trial, [^{177}Lu]Lu-PSMA-617 was administered at a dose of 7.4 GBq for 4 to 6 cycles every 6 weeks and demonstrated that adding [^{177}Lu]Lu-PSMA-617 to the standard of care improved both radiographic progression-free survival (rPFS) and overall survival (OS) [90]. Based on the findings of this trial, the European Medicines Agency and the US FDA approved [^{177}Lu]Lu-PSMA-617 for the treatment of adult PSMA-positive mCRPC patients who have previously received androgen receptor pathway inhibitors (ARPIs) and taxane-based chemotherapy [28].

However, based on toxicity observation, the [^{177}Lu]Lu-PSMA-617 group discovered higher side effects, with 52.7% having grade ≥ 3 adverse occurrences and involving 23.4% with hematological toxicity compared to 38.0% and 6.8% in the standard care group. Mild dry mouth (grade < 3) was experienced by 39.3% of patients in the [^{177}Lu]Lu-PSMA-617 group, compared to 1.0% in the standard care group [16, 86]. This adverse effect is largely caused by high radiation doses administered frequently [9]. Therefore, for future development, it is necessary to create a delivery system that increases the effective dose of [^{177}Lu]Lu-PSMA-based radiopharmaceuticals while also combining it with other therapeutic strategies that have a synergistic effect, increasing therapeutic efficacy.

Discussion and future perspectives

sPSMAi-RLT based on α-emitting radionuclides, represented by [^{225}Ac]Ac-PSMA-617, and sPSMAi-RLT based on β^--emitting radionuclides, represented by [^{177}Lu]Lu-PSMA-617, have both been clinically proven to be effective in treating mCRPC [55, 91]. However, both have negative side effects such as xerostomia and other potential toxicities as a result of the high radiation doses administered frequently during mCRPC treatment [9, 21]. As a result, an innovative approach is required to improve the efficacy of sPSMAi-RLT-based mCRPC therapy while minimizing potential negative side effects. sPSMAi-RLT agents can be developed or modified using the structure of [^{225}Ac]Ac-PSMA-617/[^{177}Lu]Lu-PSMA-617, which is made up of a binding motif, a radiolabeled moiety (chelator), and a linker [22]. Among the three components, modifying the linker

has the greatest potential to improve sPSMAi-RLT efficacy. A linker in the sPSMAi-RLT agent is essential for bridging between a binding motif and a chelator, as well as sustaining peptide affinity for the receptor and avoiding steric hindrance [92]. It can induce a variety of effects by altering the size, shape, solubility, stability, and molecular weight of chemical structures to improve metabolic stability and modulate biodistribution [93].

Modifying the linker may improve the therapeutic potential of sPSMAi-RLT by influencing its pharmacokinetic properties [26]. Benesová et al. found that both in vitro and in vivo experiments with 18 synthetic PSMA inhibitor variants revealed that structured chemical modification of the linker has significant effects on the in vivo tumor-targeting and pharmacokinetic properties, including cellular uptake, PSMA inhibition potencies, and biodistribution behavior of the DOTA conjugates [94]. In their study, Liu et al. discovered that utilizing the right linker is critical in the development of PSMA detection probes and therapeutic agents that specifically target PSMA-overexpressing cells [95]. Therefore, modifying the linker that bridges the DOTA chelator and the Glu-urea-Lys binding motif opens up novel opportunities for increasing the efficacy of prostate cancer therapy through the development of a new sPSMAi-RLT agent.

Nanoparticles, which have been extensively researched in recent years for use as therapeutic agents, diagnostics, and drug delivery systems [38, 96, 97], hold great promise as linker candidates in the development of sPSMAi-RLT agents. One of the most significant effects of nanoparticles' small size in biological systems is increased permeability and retention, as well as the high surface-to-volume ratio, which allows for the implementation of various desired manipulations [38]. Many types of biocompatible polymer nanoparticles, such as dendrimers, can potentially be applied as a linker. However, they are not heat stable and cannot withstand the high radiolabeling temperatures required to perform radionuclide chelation [36]. The role of the linker can be replaced by AuNPs, which are resistant to high temperatures. In terms of TRLT, AuNPs, particularly those with spherical morphology, have the advantage of efficiently transporting the total dose of radioactivity to cancer cells [35]. This is because of their large surface area, which allows for the binding of multiple radioligands and targeting molecules [35, 97].

Dziawer et al. reported a study on AuNPs labeled with ^{211}At, utilizing [^{211}At]At-AuNP-PEG-Trastuzumab as a therapeutic agent in the HER2-overexpressing human ovarian SKOV-3 cell line [98]. The findings indicated that the cytotoxic efficacy of [^{211}At]At-AuNP-PEG-Trastuzumab is sevenfold superior to that of [^{177}Lu]Lu-DOTA-Trastuzumab, although the 22-fold shorter half-life of ^{211}At relative to ^{177}Lu [98, 99]. These results demonstrate a heightened therapeutic efficacy of decorated AuNPs in comparison to free ligands. Another advantage of using gold nanospheres in therapeutic applications is their photostability, resistance to light bleaching, low toxicity, and ease of bioconjugation, which allows them to accumulate precisely in tumor cells and cause local hyperthermia [97, 100]. This hyperthermia heat can accelerate intratumoral blood flow, resulting in enhanced oxygen levels in the tumor microenvironment and allowing it to overcome hypoxia [101], thereby potentially reducing the resistance of cancer cells to sPSMAi-RLT. However, no study has been conducted to date on the development and testing of sPSMAi-RLT agents that use AuNS as a linker to improve the efficacy of mCRPC treatment.

In summary, future research on sPSMAi-RLT agents using gold nanoparticles for the treatment of mCRPC is essential, and it should address appropriate AuNP synthesis methods for therapeutic purposes, strategies for radiolabeling and conjugation of small molecule PSMA inhibitors to AuNPs, radiobiology and dosimetry, and potential combination with photothermal therapy to improve therapeutic efficacy.

Development of spherical AuNPs for therapeutic purposes

Traditional AuNP synthesis methods frequently use toxic substances such as strong acids and unsafe reducing agents, which are harmful to the environment and human health [97]. Although the Brust-Schiffrin method can produce AuNPs with controlled spherical size and low polydispersity, there are still some concerns, such as the use of $NaBH_4$, which is toxic and unsuitable for therapeutic purposes, leading to additional purification processes that may reduce yield [96, 102]. As a result, a more convenient and safe synthesis method is required to overcome the limitations of the previous one. The phytosynthesis method using plant extract for spherical AuNP production provides multiple benefits, such as a facile method, eco-friendliness, lower toxicity, facilitation of a controlled synthesis with a well-defined size as well as good stability, and less likelihood of causing adverse reactions when dealing with biological systems, making them particularly useful in medical applications such as medicine delivery as well as cancer therapy [97, 102, 103]. Furthermore, plant extracts consisting of biological compounds with high antioxidant activity can significantly improve the pharmacological effects of cancer treatment [104].

Plant extracts can replace reducing agents and synthetic chemical stabilizers or capping agents that are toxic and less biocompatible, eliminating the need for a complicated and imperfect separation process at the end of the synthesis process. Polyphenols, flavonoids, and alkaloids are biomolecules derived from plant extracts that play an important role in the bioreduction and stabilization of AuNPs [105]. The

toxicity of AuNPs may differ depending on their size and surface composition. Smaller nanoparticles may be more poisonous because they can penetrate cells more easily. To reduce the risk of toxicity, surface modifications such as covering AuNPs with biocompatible compounds can be applied. The phytochemicals extracted from plant parts can act as natural capping agents, covering the surface of AuNPs in biocompatible materials, increasing their stability and biocompatibility while decreasing AuNP toxicity [97, 106].

Good stability is an important consideration when developing nanoparticle synthesis methods for therapeutic applications, particularly if the preparation is for intravenous injection [107, 108]. In the phytosynthesis method using plant extracts, the reaction temperature and plant extract concentration have a direct impact on nanoparticle stability [105, 109]. Applying a reaction temperature of 30°C–60°C can quickly convert gold ions into gold atoms, resulting in smaller, more uniform particles. However, a further increase in reaction temperature causes the formation of larger nanoparticles with a high polydispersity. This is due to the aggregation of nanoparticles caused by the extremely high reduction rate, which prevents the capping of newly generated particles and causes particle agglomeration [105, 110]. Utilization of low concentrations of plant extracts results in the formation of nanoparticles with anisotropic forms and large and non-uniform particle sizes, indicating that the low quantity of plant extracts is ineffective in capping particles and is unable to prevent particle aggregation or agglomeration, resulting in poor stability of the nanoparticles. In contrast, the higher concentration of plant extracts used promotes the formation of nanoparticles with smaller and more uniform sizes and improved stability [111].

Based on the information above, our research group developed a phytosynthesis method for [^{198}Au]AuNPs using an aqueous extract of turmeric rhizome (*Curcuma longa*) at a reaction temperature of 60°C, resulting in AuNPs with uniform spherical morphology and an average particle diameter of 41 nm, which remained stable for 14 days [102]. This stability is greater than that of the traditional method for synthesizing [^{198}Au]AuNPs using citrate as a reducing and capping agent, which only remained stable for 7 days [112]. The presence of alkaloids and phenolic groups in *C. longa* rhizome extract served as a capping agent, stabilizer, or template, while flavonoids, which have strong antioxidant properties, served as a reducing agent for the reduction of Au^{3+} ions to Au^0 in the formation of spherical AuNPs [102].

Radiolabeling and small-molecule PSMA inhibitor conjugation of AuNPs

Radionuclide degradation from the radio-conjugate due to the in vivo instability can result in its accumulation in non-targeted tissues. Consequently, establishing a stable link between the radionuclide and AuNPs is critical for the successful use of radiolabeled AuNPs in cancer therapy [35, 96]. In this context, there are several synthetic methods able to functionalize AuNPs, including (i) using bifunctional chelators that attach to AuNPs via thiolated linkers or a covalent bond to the vector molecule in the AuNP's surface [36, 113]; (ii) directly conjugating amino/thiolated molecules to preformed AuNP surfaces [114]; and (iii) chemical modifications of molecules that are existing in the AuNP structure [96, 115]. The most frequent one of these strategies is the use of bifunctional chelators, which form strong complexes with radiometals [35]. In radiopharmaceutical development, an effective bifunctional chelator reduces the dissociation of radionuclides from the chelator in vivo, thereby preventing the trans-chelation of the radiometallic ion, which could result in radioisotope accumulation in non-target tissues. This is determined by the bifunctional chelator's thermodynamic stability (direction of dissociation reaction) and kinetic inertness (rate of dissociation reaction) [35, 116].

The success of radiolabeling of AuNPs can be determined through radiochemical yield and radiochemical purity. The radiochemical yield is the amount of activity in the product expressed as a percentage of the initial activity and a high radiochemical yield is necessary to achieve high specific activity, which is ideal for therapeutic applications [116, 117]. Meanwhile, radiochemical purity measures the presence of other radionuclides in a radiopharmaceutical sample, and high radiochemical purity is a key characteristic of radiolabeled nanopharmaceutical products used as diagnostic or therapeutic agents [35]. The radiochemical yield of radionuclides attached to AuNPs via bifunctional chelators can range from 30% to > 90%, while the radiochemical purity after purification remains greater than 95% [35, 118, 119].

The radiolabeling of AuNPs with a bifunctional chelator can be accomplished through two methods: attaching the chelator to the nanoparticle surface before coupling with the radioisotope, or coordinating the radiometal with the bifunctional chelator and subsequently binding the complex to the AuNPs [128]. Our research group has started a preliminary study on radiolabeling AuNP-PEG-Lys-urea-Glu with the [^{177}Lu]Lu-DOTA complex, using PEG linkers with terminal-free thiols, yielding satisfactory radiochemical efficiency. The resulting radioconjugate was further purified to a radiochemical purity of more than 95% (data not shown). The method of functionalizing AuNPs with PEG linkers containing terminal-free thiols that readily bind to Au has been widely used to generate highly stable Au–S bonds, especially for AuNP radiolabeling, as shown in Table 3. The other side of the PEG linker can be modified by conjugation with a chelator or a chemical group capable of conjugating with a targeting moiety [36, 129].

Given the significance of interactions with plasma proteins in the biological fate of nanoparticles, it is essential

Table 3 Study of AuNP radiolabeling for therapeutic application

Radio-conjugate	AuNP morphology	Linker/ Targeting moiety	Study results	References
[^{177}Lu]Lu-DOTA-Gly-Gly-Cys-AuNP-cyclo(Arg-Gly-Asp-D-Phe-Lys)Cys	Nanosphere with a particle size of 20 nm	Gly-Gly-Cys/ cyclo(Arg-Gly-Asp-D-Phe-Lys)Cys	In vivo studies utilizing athymic mouse models with glioma tumors treated with [^{177}Lu]Lu-AuNPs conjugated to c(RGDfK)C demonstrated a significant reduction in tumor progression, metabolic activity, intratumoral vessels, and VEGF gene expression. Non-target organs exhibited minimal uptake, and renal toxicity was not induced, demonstrating favorable characteristics for targeted radionuclide therapy in tumors expressing $\alpha(\nu)\beta(3)$ integrins	[120, 121]
[^{177}Lu]Lu-DOTA-PEG-AuNP-PEG-Panitumumab	Nanosphere with a particle size of 30 nm	OPSS-PEG-DOTA, OPSS-PEG-succinimidyl valerate (SVA)/ Panitumumab	[^{177}Lu]Lu-DOTA-PEG-AuNP-PEG-Panitumumab injected intratumorally was extremely effective in inhibiting the growth of breast cancer tumors in CD-1 athymic mice while causing no normal organ damage	[122]
[^{177}Lu]Lu-DOTA-PEG-AuNP-PEG-Trastuzumab	Nanosphere with a particle size of 30 nm	OPSS-PEG$_{3k}$-DOTA/ Trastuzumab	[^{177}Lu]LuDOTA-PEG-AuNP-PEG-Trastuzumab (3 MBq; 0.15 mg; 5.5×10^{11} AuNP) was administered intratumorally in NOD/SCID mice bearing subcutaneously implanted MDA-MB-361 human breast cancer xenografts. This treatment resulted in a significant reduction in tumor growth over 16 days when compared to control mice receiving normal saline injections	[123]
[^{177}Lu]Lu-DOTA-PEG-AuNP-PEG- Cetuximab	Nanosphere with a particle size of 15 nm	OPSS-PEG$_{3.5\,k}$-DOTA, OPSS-PEG$_{5k}$-SVA/ Cetuximab	Treatment with [^{177}Lu]Lu-DOTA-PEG-AuNP-PEG-Cetuximab reduced colony formation in HCT8, MDA-MB-468, and HCT116 cell lines	[124]
[^{177}Lu]Lu-DOTA-GA-AuNP-2-nitroimidazole (2-NIM)	Nanosphere with an average particle size of 15 ± 1.2 nm	2,2,2-(10-(4-((2-(5-(1,2-dithiolan-3-yl) pentanamido)ethyl)amino)-1-carboxy-4-oxobutyl)-1,4,7,10-tetraazacyclododecane-1,4,7-triyl)triacetic acid (TA-DOTA-GA)/ 2-nitroimidazole (2-NIM)	In vitro studies revealed that [^{177}Lu]Lu-DOTA-GA-AuNP-2-NIM nanoparticles accumulate extremely well in CHO cells under hypoxic conditions	[125]
PEG-*p*Glu([^{177}Lu]Lu-DOTA)$_{13}$-LA$_6$-AuNP	Nanosphere with an average particle size of 23 ± 3 nm	PEG-*p*Glu(DOTA)$_{13}$-LA$_6$	PEG-*p*Glu([^{177}Lu]Lu-DOTA)$_{13}$-LA$_6$-AuNP (2.0 MBq, 4×10^{11} AuNPs) reduced clonogenic survival in U251-Luc cells, increased DNA double-strand breaks by 14.3-fold compared to cells treated with unlabeled AuNPs, and no normal tissue toxicity was observed	[126]

Table 3 (continued)

Radio-conjugate	AuNP morphology	Linker/ Targeting moiety	Study results	References
Au@TADOTAGA nanoparticles radiolabeled with ^{225}Ac	Nanosphere with an average particle size of 5–9 nm	2,2,2-(10-(4-((2-(5-(1,2-dithiolan-3-yl) pentanamido)ethyl)amino)-1-carboxy-4-oxobutyl)-1,4,7,10-tetraazacyclododecane-1,4,7-triyl)triacetic acid (TADOTAGA)	AuNPs radiolabeled with ^{225}Ac via the macrocyclic chelator TADOTAGA inhibited tumor growth after intratumoral injection in U87MG tumor-bearing mice, even though only very low activities were injected per mouse	[127]

to investigate the stability of radiolabeled AuNPs in biological media. Mittal et al. examined the in vitro stability of [^{177}Lu]Lu-DOTA-AuNP-PEG$_{2K}$-(2-NIM) nanoparticles in PBS and human serum over one week using radio-TLC. During this period, the radiochemical purity of radiolabeled AuNPs in PBS decreased slightly from 98 ± 2.5% to 96.41 ± 1.89%, while in human serum it decreased from 98.01 ± 2.68% to 94.12 ± 1.95% [125]. Luna-Gutiérrez et al. investigated the in vitro stability of [^{177}Lu]Lu-DOTA-Gly-Gly-Cys-AuNP-c[RGDfK(C)] in human serum. After 24 h, the radiochemical purity of radiolabeled AuNPs was measured at 92.0 ± 1.1%. The 522 nm surface plasmon resonance characteristic of AuNPs remained stable, with a slight shift to higher energy at 524 nm [130]. These results demonstrate the high stability of radiolabeled AuNPs in biological media. However, when exposed to heat, oxidizing agents, or other thiol-containing molecules like glutathione (GSH) or dithiothreitol (DTT), the binding of monothiol-containing ligands to AuNP becomes unstable. This can lead to instability in vivo of AuNP structures made from monothiol-containing PEG ligands [129].

One method for improving the stability of thiol-functionalized ligands binding to AuNP is to increase the number of thiols per ligand, resulting in more avid multivalent binding to the gold surface [129, 131, 132]. Yook et al. investigated the comparative stability of AuNP conjugated to a ^{177}Lu-chelating polymer via a single thiol [DOTA-PEG-orthopyridyldisulfide (OPSS)], a dithiol [DOTA-PEG-lipoic acid (LA)], and a multithiol end-group [PEG-*p*Glu(DOTA)$_8$-LA$_4$] (the structure of ^{177}Lu-chelating polymer-AuNP conjugates is shown in Fig. 3) and determined its elimination and biodistribution in mice. The in vitro stability of radiolabeled AuNPs was assessed by incubating [^{177}Lu]Lu-DOTA-PEG-OPSS-AuNP, [^{177}Lu]Lu-DOTA-PEG-LA-AuNP, and PEG-*p*Glu([^{177}Lu]Lu-DOTA)$_8$-LA$_4$-AuNP with 1 mL of human plasma at 37°C for durations of 0.2, 0.5, 1, 3, 5, 24, 48, and 72 h in low-binding microcentrifuge tubes. After 72 h in plasma, PEG-*p*Glu([^{177}Lu]Lu-DOTA)$_8$-LA$_4$ remained bound to AuNP at 59.2 ± 8.4%, while [^{177}Lu]Lu-DOTA-PEG-OPSS-AuNP and [^{177}Lu]Lu-DOTA-PEG-LA-AuNP had significantly lower binding (17.6 ± 3.1%; $P = 0.001$ and 16.6 ± 4.3%; $P = 0.001$, respectively). These results exhibited that PEG-*p*Glu([^{177}Lu]Lu-DOTA)$_8$-LA$_4$-AuNP outperformed [^{177}Lu]Lu-DOTA-PEG-LA-AuNP and [^{177}Lu]Lu-DOTA-PEG-OPSS-AuNP in terms of in vitro aggregation stability [129].

In athymic mice, PEG-*p*Glu([^{177}Lu]Lu-DOTA)$_8$-LA$_4$-AuNP and [^{177}Lu]Lu-DOTA-PEG-LA-AuNP revealed slower elimination from the body and less radioactivity excretion into the urine, indicating that these conjugates were less easily dissociated from AuNP in vivo. More than 90% of ^{177}Lu was eliminated from the body through urine, with much lower amounts excreted in feces. Furthermore,

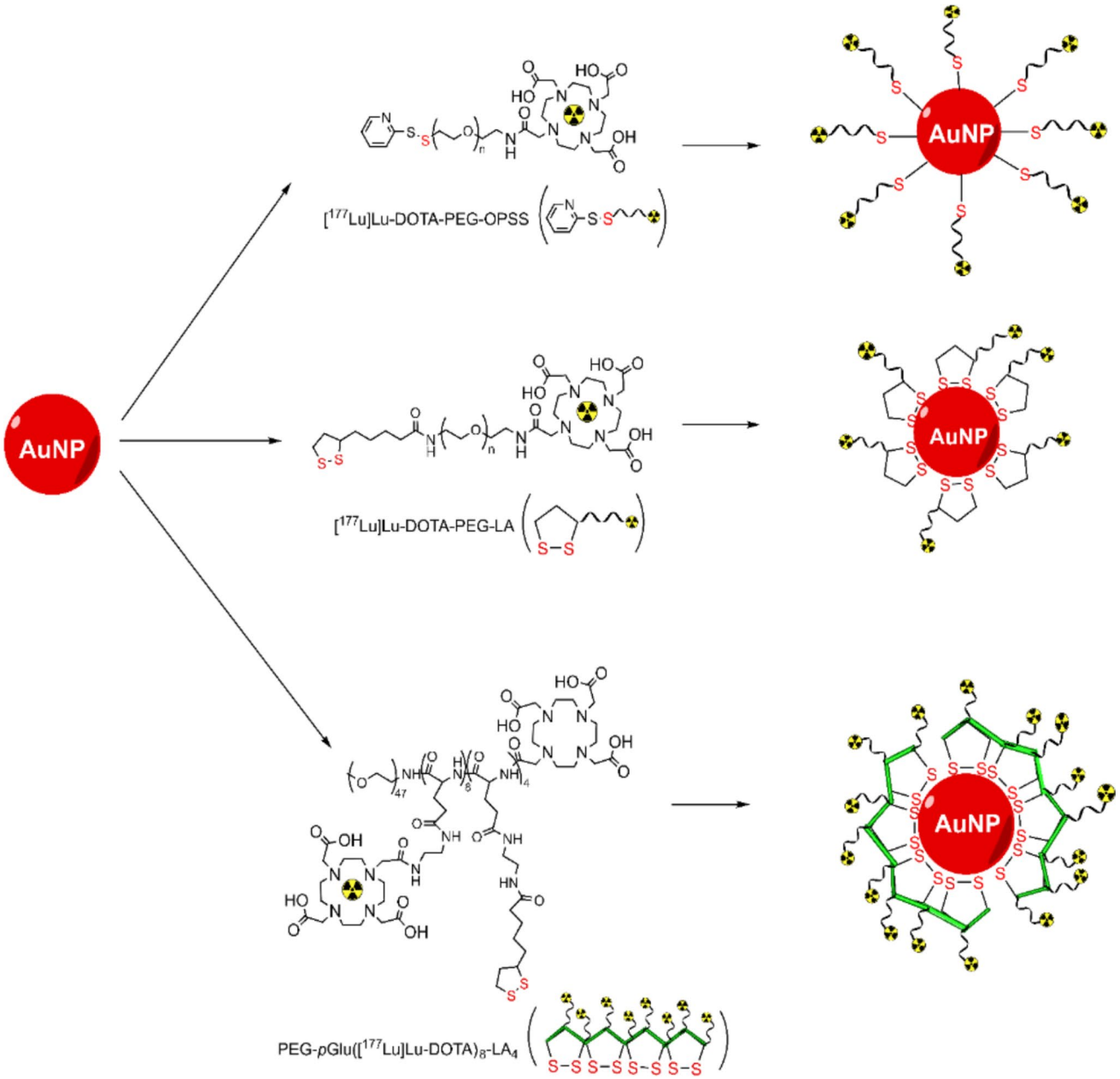

Fig. 3 Schematic depicting the formation of ^{177}Lu-chelating polymer-AuNP conjugates

PEG-*p*Glu([^{177}Lu]Lu-DOTA)$_8$-LA$_4$-AuNP had the lowest liver uptake, whereas spleen uptake was greater than [^{177}Lu]Lu-DOTA-PEG-LA-AuNP or [^{177}Lu]Lu-DOTAPEG-OPSS-AuNP [129].

These findings show that AuNP binds more strongly to multithiol end-groups, resulting in more stable conjugates than to AuNP-dithiol or AuNP-monothiol, both in vitro and in vivo. Moreover, the AuNPs radiolabeling technique utilizing bifunctional chelators has one major challenge: the trans-chelation of radiometallic ions, which may lead to radioisotope accumulation in non-target tissues.

The integration of AuNPs with PSMA-targeting ligands for prostate cancer cell-surface biomarkers is a viable framework for facilitating selective transport and absorption into target cells [40]. In contrast to antibodies, small-molecule PSMA inhibitors can be attached to nanoparticle surfaces in adjustable orientations that maintain their affinity for target prostate cancer cells [40, 133].

Kasten et al. developed and investigated the first AuNP system with a small molecule phosphoramidate peptidomimetic inhibitor for targeted administration to PSMA-expressing prostate cancer cells. The overall strategy comprised

conjugating streptavidin-coated AuNPs with a biotin-linked small-molecule PSMA inhibitor, CTT54, to create PSMA-targeted AuNPs. PSMA inhibitor-mediated binding was assessed in vitro by incubating AuNP-streptavidin–biotin-PEG_{12}-CTT54 with PSMA-positive LNCaP and PSMA-negative PC3flu cells. AuNP-streptavidin–biotin-PEG_{12}-CTT54 demonstrated significantly higher binding to LNCaP cells than that of non-targeted AuNP-streptavidin. These findings supported the idea that small-molecule PSMA inhibitors could facilitate the delivery of AuNPs to prostate cancer cells. AuNP-streptavidin–biotin-PEG_{12}-CTT54 and non-targeted AuNP-streptavidin bound significantly less to PC3flu cells than AuNP-streptavidin–biotin-PEG_{12}-CTT54 bound to LNCaP cells. Therefore, the enhanced delivery of inhibitor-targeted AuNPs in LNCaP cells was attributed to PSMA binding mediated by the inhibitor, rather than non-specific cell interactions [40].

Mangadlao et al. developed a theranostic agent using small-molecule PSMA inhibitors, PSMA-1-targeted AuNPs loaded with the fluorescent photodynamic therapy (PDT) drug Pc4. PSMA-1 is a Glu-urea-based ligand with a high binding affinity ($IC_{50} = 2.30$ nM) for the PSMA receptor. The PSMA-1 ligand was first conjugated to thiol-terminated PEG to form SH-PEG_{5k}-PSMA1, which was then grafted to the dodecylamine (DDA)-stabilized AuNPs surface via ligand exchange reaction facilitated by the strong interaction between gold and thiol. Furthermore, the amphiphilicity of PEG allows it to encapsulate water-insoluble Pc4 in the nanoparticle's corona. Pc4 loading was carried out by adding a 40-fold excess of Pc4 to a chloroform solution of AuNP-PEG_{5k}-PSMA1. Because of the amphiphilic nature of PEG, chloroform swells the corona, allowing Pc4 molecules to diffuse into the PEG coating [134]. The effectiveness of these nanoparticles against PSMA-positive PC3pip and PSMA-negative PC3flu cells was evaluated in vitro and in vivo.

In vitro cellular uptake tests were performed by incubating PSMA-expressing PC3pip cells with various concentrations of AuNP-PEG_{5k}-PSMA-1, PSMA-1, and the parent ligand, ZJ24, in the presence of 12 nM H-labeled ZJ24. A scintillation counter was used to measure radioactivity and determine cell-associated uptake. The results revealed that PSMA-positive PC3pip cells uptake AuNP-PEG_{5k}-PSMA-1 ($IC_{50} = 0.17$ nM) significantly more than PSMA-1 ($IC_{50} = 2.01$ nM). In vitro phototoxicity studies were performed by incubating PSMA-expressing PC3pip cells and nonexpressing PC3flu cells with Pc4-containing AuNP-PEG_{5k}-PSMA-1. The percentage of cell viability was determined 24 h later using the 3-(4,5-dimethylthiazol-2-yl)-5-(3carboxymethoxyphenyl)-2-(4sulfophenyl)-2H-tetrazolium (MTS) assay. Furthermore, when exposed to light at various doses of Pc4-containing AuNP-PEG_{5k}-PSMA-1, PC3pip cells showed more cell ablation than PC3flu cells, indicating active targeting followed by Pc4 delivery [134].

In vivo PDT experiments were carried out on athymic nude mice bearing a PC3pip tumor labeled with a green fluorescent protein (GFP). When tumors were large enough, the mice were injected with 0.07 mg/kg Pc4-containing AuNP-PEG5k-PSMA-1 through the tail vein. The efficacy of the treatment was assessed by measuring tumor growth with a digital caliper, GFP fluorescence by Maestro, and body weight loss 14 days after PDT. The result of in vivo PDT studies showed that treated animals experienced tumor remission 14 days after PDT, and Pc4-containing AuNP-PEG_{5k}-PSMA-1 can selectively deliver the payload that enables tumor visualization and destruction when exposed to light [134].

Luo et al. reported the conjugation of SH-PEG_{2k}-PSMA-1 with AuNP sizes of 2 nm, 5 nm, and 19 nm, and then investigated the effects of particle size and PSMA-1 ligand on cell/tumor uptake and X-ray radiotherapy efficacy. The PSMA-1 ligand is critical for increasing the specific uptake of AuNPs by PSMA-expressing PC3pip cells, regardless of particle size. However, particle size had a significant impact on the targeted AuNPs' ability to sensitize cells to X-ray radiation therapy. In vitro cellular uptake tests were performed by incubating PSMA-expressing PC3pip cells and PSMA-nonexpressing PC3flu cells with various sizes of AuNP-PEG_{5k}-PSMA-1 at an Au concentration of 60 μg/mL. The silver staining assay was used for cellular uptake assessment. In vitro studies revealed that larger targeted AuNPs (19 nm) resulted in greater gold uptake into PC3pip cells as well as less gold uptake into PC3flu cells. However, the in vivo biological studies showed that gold uptake into cells was reduced when PC3pip tumor-bearing mice were given larger AuNPs, implying that smaller AuNPs were more effective radiosensitizers. Smaller AuNPs may be more effective, as they can enter tumor cells through extravasation from the vasculature, whereas 19 nm AuNPs may not. Furthermore, smaller AuNPs reduced liver uptake, potentially reducing off-target elemental toxicity and radiation sensitivity to non-targeted tissues [135].

Wang et al. developed an ultrasmall AuNP-based contrast agent conjugated with PSMA-1 (AGGP) for use as a multimodal imaging agent. Nanoparticles approximately ~ 5 nm in size, encased in glutathione shells, exhibit colloidal stability and minimize non-specific protein adsorption. This design reduces sequestration by the mononuclear phagocyte system (liver, spleen), thereby extending circulation time and improving tumor site perfusion. Confocal microscopy, flow cytometry, and ICP-MS analyses demonstrate that AGGP exhibits preferential binding and internalization in PSMA-positive PC3pip cells relative to PSMA-negative PC3flu cells. The magnetic resonance (MR), CT, and near-infrared fluorescence (NIRF) imaging of these cells exhibit significantly enhanced signals, indicating that AGGP's targeting

strategy effectively translates from molecular design to cellular function [136].

Using mouse models implanted with PSMA-positive and negative tumors, AGGP produces robust contrast enhancement in PSMA-positive tumors across MR, CT, and NIRF modalities, persisting up to 24 h. Signal intensities correlate strongly with tumor PSMA expression and size, enabling longitudinal monitoring of tumor progression from early to advanced stages. This capability underlines AGGP's potential for non-invasive early diagnosis and treatment planning. Comprehensive toxicological evaluation, including body weight monitoring, immune cytokine assays, liver and kidney function tests, and histopathological examinations, indicates that AGGP is well-tolerated in vivo. Preferential renal clearance reduces systemic exposure and long-term retention, alleviating concerns about AuNP accumulation. This biosafety is critical for regulatory approval and patient acceptance [136].

Radiobiology and dosimetry

The present knowledge of AuNP-based sPSMAi-RLT is insufficient, highlighting the need for a coherent and systematic experimental approach to thoroughly assess the radiobiological effectiveness of AuNPs. Cell survival serves as the primary assay in radiobiology for evaluating the effectiveness of treatments and has been widely utilized to assess the influence of nanoparticles on radiation effects. This in vitro technique enables the evaluation of radiation cytotoxicity by examining the capacity of an individual cell to proliferate and form a colony [137]. Survival percentage estimation methods have been established through cell viability assays, including the methyl-thiazol-tetrazolium (MTT) assay and the trypan blue exclusion test [138, 139].

However, efforts to quantify the improvement caused by AuNPs appear to have created confusion and resulted in the definition of a large number of parameters. For this reason, the International Commission on Radiation Units and Measurements (ICRU) recommends using the whole survival curve rather than single-point measurements to evaluate changes in radiobiological effectiveness and to provide a comprehensive understanding of the dose–response relationship caused by AuNPs. Therefore, the sensitizer enhancement ratio (SER), defined as the ratio of mean inactivation dose (MID) in non-exposed cells with nanoparticle-exposed cells, appears to be an appropriate approach for providing a single parameter to quantify the impact of AuNPs on in vitro survival curves [137].

Another important step in the radiobiological study of high-Z nanoparticles is determining the amount of AuNPs taken up by cells, as well as their subcellular distribution, due to the physical and chemical changes at the nanoscale caused by AuNPs when exposed to ionizing radiation [137, 140]. Inductively coupled plasma (ICP) methods with atomic emission spectroscopy (ICP-AES) or mass spectrometry (ICP-MS) are the "gold standard" for measuring AuNPs levels in cells due to their high sensitivity and robustness for elemental analysis [137, 140, 141]. Although it is simple to convert material mass into the number of AuNPs, this needs precise information about the AuNPs' size and elemental composition, as well as an assumption of uniform distribution.

The predominant ionization events transpire within water molecules, where the indirect action of radiation, primarily facilitated by reactive oxygen species (ROS), constitutes the principal mechanism of DNA damage, particularly in the presence of low LET radiation such as β^--emitting radionuclides. In this regard, AuNPs may interact directly with incoming ionizing radiation from radionuclides, affecting the final ROS spectrum and yield [137]. Therefore, a comprehensive knowledge of the ROS production associated with AuNPs is required to address the mechanism underlying the biological response, as is an appropriate methodology for accurately and reliably measuring the yield and spectrum of ROS. There are several techniques for determining the level of ROS, including colorimetric methods, fluorescent or chemiluminescent dyes, and the coumarin assay [140, 142, 143]. Additional pathways for ROS formation in the presence of AuNPs may result in non-linearity in ROS yield as a function of dose. Reports on the relative ROS at various dose levels would therefore be recommended [137].

DNA damage has been identified as an important factor in regulating radiation response. The impact of AuNP-mediated DNA damage requires quantitative and mechanistic studies, as well as a comparison of radiation-induced DNA damage in the presence and absence of AuNPs. DNA damage can be detected through various strategies, such as the comet assay, which quantifies denatured DNA fragments that migrate out of the cell nucleus during electrophoresis, differential plasmid DNA migration on agarose gel electrophoresis, which is an established approach for quantifying single-strand breaks and double-strand breaks in simple biological systems, and immunostaining for γ-H2AX and 53BP1 foci, which provide key information on both the rate of DNA [144–146].

A large number of theoretical studies on the radio-sensitizing effects of high-Z nanoparticles employ Monte Carlo methods to assess dose distributions, develop a dosimetry model to calculate the absorbed dose of healthy tissues, and define the therapeutic window of a radiopharmaceutical, as well as estimate enhancement effects [34, 85]. Monte Carlo simulations are a highly effective instrument for investigating changes in the spatial distribution of dose deposition caused by AuNPs at the nanometer scale [34]. Several dedicated Monte Carlo simulations, including EGSnrc, Geant4, PENELOPE, MCNP5, MCNPX, and NORTEC, have been used to investigate high-Z nanoparticle radio-enhancement.

These simulations can produce useful micro-dosimetric parameters, which should then be validated against experimental data using established radiobiological models. Although Monte Carlo codes have been extensively benchmarked and validated for conventional dosimetry, their application to very low energy thresholds and nanometre–scale ranges remains subject to potentially large uncertainties. As a result, accurate estimation of physical processes requires a detailed representation of the radiation source and samples, including geometry, composition, environment, etc. [137].

Combination with photothermal therapy

Photothermal therapy (PTT) could represent a significant improvement in prostate cancer treatment largely because of its highly localized and selective cytotoxic effect, as well as its low prevalence of side effects and tumor resistance [43]. The photothermal effect is simply defined as the conversion of light energy into heat energy. Heat formation occurs when particles are irradiated with light and reach the lowest singlet excited state before returning to the ground state, resulting in resonance energy that causes synchronized oscillations of electrons, which eventually produce heat [100].

The photothermal effect requires the presence of a photothermal agent in conjunction with radiation from a light source. Photothermal agents are an essential element of this technique, with material properties such as light absorption efficiency, large cross-sectional area, excellent photothermal conversion efficiency, long-term photothermal stability, and easily performed surface modification [44, 147]. These characteristics are exhibited by noble metal nanomaterials, especially gold nanoparticles, alongside surface plasmon resonance properties [44, 102]. In the application of PTT, the processes of necrosis and apoptosis (cell death) are determined by the laser power and temperature achieved within the cancer tissue during the PTT process [46, 147, 148]. Temperature increases have a significant impact on cellular changes, as well as on tumor cells. The light source for PTT is a laser that emits visible and near-infrared light to raise the temperature of the cell or tissue environment to 41°C to 49°C, allowing cancer cells to be effectively damaged, a process known clinically as hyperthermia [102, 147]. The type of light used is determined by the location of the target organ to be treated, with visible light used for therapy of organs or tissues near the body's surface and near-infrared light (NIR) used for organs or tissues inside the body because light at this wavelength is greatly less absorbed by water molecules [44, 149].

Combination therapies offer the potential for new and more effective cancer treatments by exploiting the combined benefits of various therapeutic methods. In sPSMAi-RLT, low-energy α- and β^--particle emitter radionuclides deliver radiation doses within a short range. When targeted to prostate cancer cells, the majority of the dose is deposited within the tumor, avoiding surrounding normal tissues [36]. sPSMAi-RLT is an effective mCRPC treatment, but in hypoxia conditions, cancer cells proliferate rapidly and consume large amounts of oxygen, resulting in insufficient oxygen in the tumor microenvironment and potential resistance to this treatment [101, 150]. The combination with PTT, which can produce hyperthermia heat, can accelerate intratumoral blood flow, resulting in enhanced oxygen levels in the tumor microenvironment and allowing it to overcome hypoxia [151]. Furthermore, the hyperthermia heat generated from the photothermal effect causes a lethal effect on S-phase radio-resistant cells, thereby reducing the resistance of cancer cells to TRLT [101, 151].

Several therapeutic agents implementing a combination of PTT with β^--particle-emitting radionuclides, also known as radio-photothermal agents, have been developed and preliminary studies have been conducted regarding the synergistic effects and efficacy produced, as shown in Table 4. The findings of our previous research group revealed that the combination therapy using radioactive gold nanoparticles ([^{198}Au]AuNPs) with 980 nm laser irradiation had a higher in vitro therapeutic efficacy than radiotherapy alone using [^{198}Au]AuNPs or photothermal therapy alone using ^{197}AuNPs [102]. We have also successfully synthesized [^{198}Au]Au@SiO_2 core–shell nanoparticles as a radio-photothermal agent that demonstrated effective near-infrared absorption and caused significant cell death in LNCaP cancer cells [152]. Both research findings indicate a great potential synergistic effect in the applications of radio-photothermal therapy. Based on these findings, the development of agents that facilitate the combination of PTT with sPSMAi-RLT has great novelty potential, particularly in terms of improving mCRPC treatment efficacy while reducing adverse side effects.

Conclusion

Currently, there is a clinical need for an innovative approach to developing therapeutic agents with improved therapeutic efficacy to overcome the limitations of currently available sPSMAi-RLT. In vitro and in vivo studies have demonstrated that modifying the linker that connects the DOTA chelator and the Glu-urea-Lys binding motif can improve sPSMAi-RLT's therapeutic potential by influencing its pharmacokinetic properties. In vitro studies have shown that the combination of TRLT and PTT via AuNP, which can act as a linker, can provide a synergistic effect in increasing cancer cell death, indicating that it has great potential to improve the efficacy of mCRPC treatment when applied to the sPSMAi-RLT agents. However, in vivo studies giving substantial proof for this hypothesis are still not available, and future

Table 4 Development of β^--particle-emitting radionuclide-photothermal cancer therapeutic agents

Radio-photothermal agent	β^--particle-emitting radionuclide	Photothermal device	Efficacy investigation	References
Polyethylene glycol (PEG)-coated [^{64}Cu]CuS nanoparticles ([^{64}Cu]CuS-PEG nanoparticles)	^{64}Cu ($t_{1/2}$: 12.7 h)	980 nm wavelength laser with a power output of 2.5 W/cm^2 and laser irradiation time of 10 min	Orthotopic Hth83 anaplastic thyroid cancer (ATC) tumors in mice were inhibited by radio-photothermal therapy with [^{64}Cu]CuS-PEG nanoparticles	[153]
^{131}I-labeled PEG-coated reduced nano-graphene oxide (RGO) ([^{131}I]I-PEG-RGO)	^{131}I ($t_{1/2}$: 8.02 d)	808 nm wavelength laser with a power output of 0.5 W/cm^2 and laser irradiation time of 20 min	The BALB/c mice model with murine breast cancer (4T1) tumors treated with [^{131}I]I-PEG-RGO-mediated radio-photothermal therapy showed enhanced efficacy compared to PTT alone. In toxicology investigations, [^{131}I]I-PEG-RGO was nontoxic	[154]
^{177}Lu-labeled semiconducting polymer nanoparticle with glucose-dependent insulinotropic polypeptide (GIP) as tumor targeting group ([^{177}Lu]Lu-SPN-GIP)	^{177}Lu ($t_{1/2}$: 6.73 d)	808 nm wavelength laser with a power output of 1.0 W/cm^2 and laser irradiation time of 5 min	The BALB/c nude mice model with pancreatic tumor treatment with [^{177}Lu]Lu-SPN-GIP-mediated radio-photothermal therapy showed enhanced efficacy compared to [^{177}Lu]Lu-SPN-GIP alone	[151]
Gold-198 nanoparticles ([^{198}Au]AuNP)	^{198}Au ($t_{1/2}$: 2.7 d)	980 nm wavelength laser with a power output of 2.0 W/cm^2 and a laser irradiation time of 5 min	[^{198}Au] AuNP-mediated radio-photothermal therapy killed cancer cells more effectively and synergistically	[102]
Silica-core gold-198 nanoshells (SiO_2@[^{198}Au]Au nanoshells)	^{198}Au ($t_{1/2}$: 2.7 d)	980 nm wavelength laser with a power output of 3.0 W/cm^2	SiO_2@[^{198}Au]Au nanoshells' synergistic radio-photothermal action killed LNCaP cells better than individual therapies	[152]

studies validating the in vitro findings are required. This will provide further knowledge about the working mechanism of AuNP linker-based sPSMAi-RLT in combination with PTT, which includes dosimetry and radiobiology.

Numerous enhancements must be implemented to facilitate the transition of sPSMAi-AuNP-RLT into clinical trials. A primary challenge is to enhance tissue-selective targeting to minimize non-specific uptake in reticuloendothelial system-associated organs, including the liver, kidneys, spleen, lungs, and stomach. Furthermore, extended blood circulation is preferred, together with an appropriate high target-to-background ratio, to enhance the contrast of the targeted tissue. Ultimately, this knowledge can help design effective AuNP linker-based sPSMAi-RLT agents and future treatment strategies for mCRPC patients, leading to better outcomes.

Acknowledgements This work was supported by Coordinated Research Project (CRP) International Atomic Energy Agency (Project No. F22078).

Author contributions Sumandi Juliyato: conceptualization, performed the literature search, data analysis, writing–original draft, Rien Ritawidya: conceptualization, supervision, writing–review & editing,Ahsanal Fikri: performed the literature search, data analysis, writing–original draft, AmalRezka Putra: performed the literature search, data analysis, writing–original draft, HerlanSetiawan: performed the literature search, data analysis, writing–review & editing, Maskur:performed the literature search, data analysis, Muammar Fawwaz: supervision, writing–review & editing, Yoki Yulizar: conceptualization, supervision, writing–review & editing.

Declarations

Conflict of interests The authors declare that they have no known competing financial interests or personalrelationships that could have appeared to influence the work reported in this paper.

References

1. Seifert R, Alberts IL, Afshar-Oromieh A, Rahbar K (2021) Prostate cancer theranostics: PSMA targeted therapy. PET Clin 16:391–396
2. Bray F, Laversanne M, Sung H et al (2024) Global cancer statistics 2022: GLOBOCAN estimates of incidence and mortality worldwide for 36 cancers in 185 countries. CA Cancer J Clin 74:229–263. https://doi.org/10.3322/caac.21834
3. Siegel RL, Kratzer TB, Giaquinto AN et al (2025) Cancer statistics, 2025. CA Cancer J Clin 75:10–45. https://doi.org/10.3322/caac.21871
4. Chen D, Hu Y (2023) Approaches for boosting antitumor immunity in prostate cancer therapy: a comprehensive review on drugs, products, and nanoparticles. J Drug Deliv Sci Technol. https://doi.org/10.1016/j.jddst.2023.105048
5. Yechiel Y, Chicheportiche A, Keidar Z, Ben-Haim S (2024) Prostate cancer radioligand therapy: beta-labeled radiopharmaceuticals. PET Clin 19:389–399
6. Liolios C, Koutsikou TS, Salvanou EA et al (2022) Synthesis and in vitro proof-of-concept studies on bispecific iron oxide magnetic nanoparticles targeting PSMA and GRP receptors for PET/MR imaging of prostate cancer. Int J Pharm. https://doi.org/10.1016/j.ijpharm.2022.122008
7. Chen M, Cai L, Xiang Y et al (2023) Advances in non-radioactive PSMA-targeted small molecule-drug conjugates in the treatment of prostate cancer. Bioorg Chem. https://doi.org/10.1016/j.bioorg.2023.106889
8. Schmidt-Hegemann NS, Zamboglou C, Mason M et al (2023) Estro-acrop recommendations for evidence-based use of androgen deprivation therapy in combination with external-beam radiotherapy in prostate cancer. Radiother Oncol. https://doi.org/10.1016/j.radonc.2023.109544
9. Hébert K, Bodin-Cufi P, Fersing C, Deshayes E (2024) New drugs for targeted radionuclide therapy in metastatic prostate cancer. Eur Urol Focus. https://doi.org/10.1016/j.euf.2024.07.016
10. Juzeniene A, Stenberg VY, Bruland ØS, Larsen RH (2021) Preclinical and clinical status of PSMA-targeted alpha therapy for metastatic castration-resistant prostate cancer. Cancers (Basel) 13:1–25
11. Nguyen CB, Alva AS (2023) The future of radioligand therapies in metastatic castrate-resistant prostate cancer. Adv Oncol 3:129–136. https://doi.org/10.1016/j.yao.2023.01.009
12. Shen CJ, Minn I, Hobbs RF et al (2020) Auger radiopharmaceutical therapy targeting prostate-specific membrane antigen in a micrometastatic model of prostate cancer. Theranostics 10:2888–2896. https://doi.org/10.7150/thno.38882
13. Elliyanti A (2022) Radiopharmaceuticals in modern cancer therapy. Radiopharmaceutic-Curr Res Better Diagn Ther. https://doi.org/10.5772/intechopen.99334
14. Buchegger F, Perillo-Adamer F, Dupertuis YM, Bischof Delaloye A (2006) Auger radiation targeted into DNA: a therapy perspective. Eur J Nucl Med Mol Imaging 33:1352–1363
15. Jones W, Griffiths K, Barata PC, Paller CJ (2020) PSMA theranostics: review of the current status of PSMA-targeted imaging and radioligand therapy. Cancers (Basel). https://doi.org/10.3390/cancers12061367
16. Song H, Guja KE, Iagaru A (2022) PSMA theragnostics for metastatic castration resistant prostate cancer. Transl Oncol. https://doi.org/10.1016/j.tranon.2022.101438
17. Adekiya TA, Hudson T, Bakare O et al (2024) PSMA-targeted combination brusatol and docetaxel nanotherapeutics for the treatment of prostate cancer. Biomed Pharmacother. https://doi.org/10.1016/j.biopha.2024.117125
18. Kahn D, Austin JC, Maguire RT et al (1999) A phase II study of [90Y] yttrium-capromab pendetide in the treatment of men with prostate cancer recurrence following radical prostatectomy. Cancer Biother Radiopharm. https://doi.org/10.1089/cbr.1999.14.99
19. Tagawa ST, Milowsky MI, Morris M et al (2013) Phase II study of lutetium-177-labeled anti-prostate-specific membrane antigen monoclonal antibody J591 for metastatic castration-resistant prostate cancer. Clin Cancer Res 19:5182–5191. https://doi.org/10.1158/1078-0432.CCR-13-0231
20. Bander NH, Nanus DM, Milowsky MI et al (2003) Targeted Systemic Therapy of Prostate Cancer With a Monoclonal Antibody to Prostate-Specific Membrane Antigen. Semin Oncol 30:667–676. https://doi.org/10.1053/S0093-7754(03)00358-0
21. Ndlovu H, Mokoala KMG, Lawal I et al (2024) Prostate-specific membrane antigen: Alpha-labeled radiopharmaceuticals. PET Clin 19:371–388
22. Alati S, Singh R, Pomper MG et al (2023) Preclinical development in radiopharmaceutical therapy for prostate cancer. Semin Nucl Med 53:663–686
23. Ritawidya R, Wongso H, Effendi N et al (2023) Lutetium-177-labeled prostate-specific membrane antigen-617 for

molecular imaging and targeted radioligand therapy of prostate cancer. Adv Pharm Bull 13:701–711
24. Martin S, Tönnesmann R, Hierlmeier I et al (2021) Identification, characterization, and suppression of side products formed during the synthesis of [177Lu]Lu-PSMA-617. J Med Chem 64:4960–4971. https://doi.org/10.1021/acs.jmedchem.1c00045
25. Weineisen M, Schottelius M, Simecek J et al (2015) 68Ga-and 177Lu-labeled PSMA i and T: optimization of a PSMA-targeted theranostic concept and first proof-of-concept human studies. J Nucl Med 56:1169–1176. https://doi.org/10.2967/jnumed.115.158550
26. Benesová M, Schäfer M, Bauder-Wüst U et al (2015) Preclinical evaluation of a tailor-made DOTA-conjugated PSMA inhibitor with optimized linker moiety for imaging and endoradiotherapy of prostate cancer. J Nucl Med 56:914–920. https://doi.org/10.2967/jnumed.114.147413
27. Kumar KSA, Mathur A (2022) A convenient total synthesis of PSMA-617: a prostate specific membrane antigen (PSMA) ligand for prostate cancer endotherapeutic applications. Eur J Medic Chem Rep. https://doi.org/10.1016/j.ejmcr.2022.100084
28. Giunta EF, Brighi N, Gurioli G et al (2024) 177Lu-PSMA therapy in metastatic prostate cancer: an updated review of prognostic and predictive biomarkers. Cancer Treat Rev. https://doi.org/10.1016/j.ctrv.2024.102699
29. Chakraborty S, Chakravarty R, Shetty P et al (2016) Prospects of medium specific activity ^{177}Lu in targeted therapy of prostate cancer using ^{177}Lu-labeled PSMA inhibitor. J Labelled Comp Radiopharm. https://doi.org/10.1002/jlcr.3414
30. Banerjee SR, Pullambhatla M, Shallal H et al (2011) A modular strategy to prepare multivalent inhibitors of prostate-specific membrane antigen (PSMA). Oncotarget 2:1244
31. Hennrich U, Eder M (2022) [177Lu]Lu-PSMA-617 (PluvictoTM): The First FDA-Approved Radiotherapeutical for Treatment of Prostate Cancer. Pharmaceuticals 15(10):1292
32. Guo J, O'Driscoll CM, Holmes JD, Rahme K (2016) Bioconjugated gold nanoparticles enhance cellular uptake: a proof of concept study for siRNA delivery in prostate cancer cells. Int J Pharm 509:16–27. https://doi.org/10.1016/j.ijpharm.2016.05.027
33. Chen Y, Yang J, Fu S, Wu J (2020) Gold nanoparticles as radiosensitizers in cancer radiotherapy. Int J Nanomedicine 15:9407–9430
34. Hainfeld JF, Dilmanian FA, Slatkin DN, Smilowitz HM (2010) Radiotherapy enhancement with gold nanoparticles. J Pharm Pharmacol 60:977–985. https://doi.org/10.1211/jpp.60.8.0005
35. Daems N, Michiels C, Lucas S et al (2021) Gold nanoparticles meet medical radionuclides. Nucl Med Biol 100–101:61–90
36. Cabello G, Nwoko KC, Mingarelli M et al (2018) Physicochemical tools: toward a detailed understanding of the architecture of targeted radiotherapy nanoparticles. ACS Appl Bio Mater 1:1639–1646. https://doi.org/10.1021/acsabm.8b00476
37. Sarkis M, Ghanem E, Rahme K (2019) Jumping on the bandwagon: a review on the versatile applications of gold nanostructures in prostate cancer. Int J Mol Sci. https://doi.org/10.3390/ijms20040970
38. Hosseini SA, Kardani A, Yaghoobi H (2023) A comprehensive review of cancer therapies mediated by conjugated gold nanoparticles with nucleic acid. Int J Biol Macromol. https://doi.org/10.1016/j.ijbiomac.2023.127184
39. Hara D, Tao W, Schmidt RM et al (2022) Boosted radiation bystander effect of PSMA-targeted gold nanoparticles in prostate cancer radiosensitization. Nanomaterials. https://doi.org/10.3390/nano12244440
40. Kasten BB, Liu T, Nedrow-Byers JR et al (2013) Targeting prostate cancer cells with PSMA inhibitor-guided gold nanoparticles. Bioorg Med Chem Lett 23:565–568. https://doi.org/10.1016/j.bmcl.2012.11.015
41. Male KB, Lachance B, Hrapovic S et al (2008) Assessment of cytotoxicity of quantum dots and gold nanoparticles using cell-based impedance spectroscopy. Anal Chem 80:5487–5493. https://doi.org/10.1021/ac8004555
42. Pan S, Sahu BK, Dhara S et al (2022) Growing AuNRs in a single step with NIR plasmon for superior SERS and plasmonic photothermal performance. J Phys Chem Solids. https://doi.org/10.1016/j.jpcs.2021.110421
43. Ferroni C, Del Rio A, Martini C et al (2019) Light-induced therapies for prostate cancer treatment. Front Chem. https://doi.org/10.3389/fchem.2019.00719
44. Kumar AVP, Dubey SK, Tiwari S et al (2021) Recent advances in nanoparticles mediated photothermal therapy induced tumor regression. Int J Pharm 606:120848
45. El-Sayed MA (2001) Some interesting properties of metals confined in time and nanometer space of different shapes. Acc Chem Res 34:257–264. https://doi.org/10.1021/ar960016n
46. Sun H, Zhang Q, Li J et al (2021) Near-infrared photoactivated nanomedicines for photothermal synergistic cancer therapy. Nano Today. https://doi.org/10.1016/j.nantod.2020.101073
47. Pakravan A, Salehi R, Mahkam M (2021) Comparison study on the effect of gold nanoparticles shape in the forms of star, hallow, cage, rods, and Si-Au and Fe-Au core-shell on photothermal cancer treatment. Photodiagnosis Photodyn Ther. https://doi.org/10.1016/j.pdpdt.2020.102144
48. King AP, Lin FI, Escorcia FE (2021) Why bother with alpha particles? Eur J Nucl Med Mol Imaging 49:7–17. https://doi.org/10.1007/s00259-021-05431-y
49. Kozempel J, Mokhodoeva O, Vlk M (2018) Progress in targeted alpha-particle therapy. What we learned about recoils release from in vivo generators. Molecules 23(3):581
50. Edem PE, Fonslet J, Kjær A et al (2016) In vivo radionuclide generators for diagnostics and therapy. Bioinorg Chem Appl. https://doi.org/10.1155/2016/6148357
51. Sathekge M, Knoesen O, Meckel M et al (2017) 213Bi-PSMA-617 targeted alpha-radionuclide therapy in metastatic castration-resistant prostate cancer. Eur J Nucl Med Mol Imaging 44:1099–1100. https://doi.org/10.1007/s00259-017-3657-9
52. Kratochwil C, Schmidt K, Afshar-Oromieh A et al (2018) Targeted alpha therapy of mCRPC: dosimetry estimate of 213Bismuth-PSMA-617. Eur J Nucl Med Mol Imaging 45:31–37. https://doi.org/10.1007/s00259-017-3817-y
53. Kratochwil C, Bruchertseifer F, Giesel FL et al (2016) 225Ac-PSMA-617 for PSMA-targeted a-radiation therapy of metastatic castration-resistant prostate cancer. J Nucl Med 57:1941–1944. https://doi.org/10.2967/jnumed.116.178673
54. Kratochwil C, Bruchertseifer F, Rathke H et al (2018) Targeted a-therapy of metastatic castration-resistant prostate cancer with 225 Ac-PSMA-617: swimmer-plot analysis suggests efficacy regarding duration of tumor control. J Nucl Med 59:795–802. https://doi.org/10.2967/jnumed.117.203539
55. Ballal S, Yadav MP, Satapathy S et al (2023) Long-term survival outcomes of salvage [225Ac]Ac-PSMA-617 targeted alpha therapy in patients with PSMA-expressing end-stage metastatic castration-resistant prostate cancer: a real-world study. Eur J Nucl Med Mol Imaging 50:3777–3789. https://doi.org/10.1007/s00259-023-06340-y
56. Favaretto C, Grundler PV, Talip Z et al (2024) Terbium-149 production: a focus on yield and quality improvement towards preclinical application. Sci Rep. https://doi.org/10.1038/s41598-024-53610-2
57. Umbricht CA, Köster U, Bernhardt P et al (2019) Alpha-PET for prostate cancer: preclinical investigation using 149Tb-PSMA-617. Sci Rep. https://doi.org/10.1038/s41598-019-54150-w

58. Stenberg VY, Larsen RH, Ma LW et al (2021) Evaluation of the psma-binding ligand212pb-ng001 in multicellular tumour spheroid and mouse models of prostate cancer. Int J Mol Sci. https://doi.org/10.3390/ijms22094815
59. Stenberg VY, Juzeniene A, Chen Q et al (2020) Preparation of the alpha-emitting prostate-specific membrane antigen targeted radioligand [212Pb]Pb-NG001 for prostate cancer. J Labelled Comp Radiopharm 63:129–143. https://doi.org/10.1002/jlcr.3825
60. Vaidyanathan G, Mease RC, Minn I et al (2021) Synthesis and preliminary evaluation of 211At-labeled inhibitors of prostate-specific membrane antigen for targeted alpha particle therapy of prostate cancer. Nucl Med Biol 94:67–80. https://doi.org/10.1016/j.nucmedbio.2021.01.002
61. Abou DS, Thiele NA, Gutsche NT et al (2021) Towards the stable chelation of radium for biomedical applications with an 18-membered macrocyclic ligand. Chem Sci 12:3733–3742. https://doi.org/10.1039/d0sc06867e
62. Banerjee SR, Lisok A, Minn I et al (2021) Preclinical evaluation of 213Bi- and 225Ac-labeled low- molecular-weight compounds for radiopharmaceutical therapy of prostate cancer. J Nucl Med 62:980–988. https://doi.org/10.2967/jnumed.120.256388
63. Ling SW, van der Veldt AA, Konijnenberg M et al (2024) Evaluation of the tolerability and safety of [225Ac]Ac-PSMA-I&T in patients with metastatic prostate cancer: a phase I dose escalation study. BMC Cancer. https://doi.org/10.1186/s12885-024-11900-y
64. Muniz M, Loprinzi CL, Orme JJ et al (2024) Salivary toxicity from PSMA-targeted radiopharmaceuticals: what we have learned and where we are going. Cancer Treat Rev. https://doi.org/10.1016/j.ctrv.2024.102748
65. Sathekge M, Bruchertseifer F, Knoesen O et al (2019) 225Ac-PSMA-617 in chemotherapy-naive patients with advanced prostate cancer: a pilot study. Eur J Nucl Med Mol Imaging 46:129–138. https://doi.org/10.1007/s00259-018-4167-0
66. Pelletier K, Côté G, Fallah-Rad N et al (2021) CKD after 225Ac-PSMA617 therapy in patients with metastatic prostate cancer. Kidney Int Rep 6:853–856. https://doi.org/10.1016/j.ekir.2020.12.006
67. Feuerecker B, Tauber R, Knorr K et al (2021) Activity and Adverse Events of Actinium-225-PSMA-617 in Advanced Metastatic Castration-resistant Prostate Cancer After Failure of Lutetium-177-PSMA[Formula presented]. Eur Urol 79:343–350. https://doi.org/10.1016/j.eururo.2020.11.013
68. Sathekge M, Bruchertseifer F, Vorster M et al (2022) mCRPC patients receiving 225Ac-PSMA-617 therapy in the post-androgen deprivation therapy setting: response to treatment and survival analysis. J Nucl Med 63:1496–1502. https://doi.org/10.2967/jnumed.121.263618
69. Gudkov SV, Shilyagina NY, Vodeneev VA, Zvyagin AV (2016) Targeted radionuclide therapy of human tumors. Int J Mol Sci 17(1):33
70. Asadian S, Mirzaei H, Kalantari BA et al (2020) β-radiating radionuclides in cancer treatment, novel insight into promising approach. Pharmacol Res. https://doi.org/10.1016/j.phrs.2020.105070
71. Lau J, Lee H, Rousseau J et al (2022) Application of cleavable linkers to improve therapeutic index of radioligand therapies. Molecules. https://doi.org/10.3390/molecules27154959
72. Gomes AR, Abrantes AM, Brito AF et al (2015) Influence of P53 on the radiotherapy response of hepatocellular carcinoma. Clin Mol Hepatol 21:257–267. https://doi.org/10.3350/cmh.2015.21.3.257
73. Sgouros G, Bodei L, McDevitt MR, Nedrow JR (2020) Radiopharmaceutical therapy in cancer: clinical advances and challenges. Nat Rev Drug Discov 19:589–608
74. Dash A, Pillai MRA, Knapp FF (2015) Production of ^{177}Lu for targeted radionuclide therapy: available options. Nucl Med Mol Imaging 49:85–107
75. Baranyai Z, Tircsó G, Rösch F (2020) The use of the macrocyclic chelator DOTA in radiochemical separations. Eur J Inorg Chem 2020:36–56
76. Banerjee S, Pillai MRA, Knapp FF (2015) Lutetium-177 therapeutic radiopharmaceuticals: linking chemistry, radiochemistry, and practical applications. Chem Rev 115:2934–2974. https://doi.org/10.1021/cr500171e
77. Wongso H, Humani TS et al (2024) Development of polyethylene glycol-modified gold nanoparticles for the delivery of Lutetium-177- radiopharmaceuticals based on antibodies. J Drug Deliv Sci Technol 100:106104
78. Ramli M, Hidayat B, Rustendi CT et al (2012) In Vitro and In Vivo testing of 177Lu-DOTA-nimotuzumab, a potential radioimmunotherapeutical agent of cancers. ITB J Sci 44(4):333–345. https://doi.org/10.5614/itbj.sci.2012.44.4.4
79. Ramli M, Hidayat B, Aguswarini S et al (2012) Preclinical Study of 177 Lu-DOTA-Trastuzumab: A Potential Radiopharmaceutical for Therapy of Breast Cancer Positive HER-2 (Uji Preklinis 177 Lu-DOTA-Trastuzumab: Radiofarmaseutika Potensial untuk Terapi Kanker Payudara HER-2 Positif). J Ilmu Kefarmasian Indonesia 11:116–122
80. Wieczorek Villas Boas CA, de Jesus Silva J, Pereira Dias LA et al (2022) In vitro and in vivo response of PSMA-617 radiolabeled with CA and NCA lutetium-177. Appl Radiat Isot. https://doi.org/10.1016/j.apradiso.2021.110064
81. Rathke H, Flechsig P, Mier W et al (2019) Dosimetry estimate and initial clinical experience with 90Y-PSMA-617. J Nucl Med 60:806–811. https://doi.org/10.2967/jnumed.118.218917
82. Kiess AP, Minn I, Chen Y et al (2015) Auger radiopharmaceutical therapy targeting prostate-specific membrane antigen. J Nucl Med 56:1401–1407. https://doi.org/10.2967/jnumed.115.155929
83. Kelly JM, Ponnala S, Amor-Coarasa A et al (2020) Preclinical evaluation of a high-affinity sarcophagine-containing PSMA ligand for 64Cu/67Cu-based theranostics in prostate cancer. Mol Pharm 17:1954–1962. https://doi.org/10.1021/acs.molpharmaceut.0c00060
84. Morgat C, Van de Voorde M, Bodin S et al (2023) Opportunities and challenges for targeted radionuclide therapy of prostate cancer using 161Tb. Medecine Nucleaire 47:333–338
85. Wenker STM, van Lith SAM, Tamborino G et al (2025) The potential of targeted radionuclide therapy to treat hypoxic tumor cells. Nucl Med Biol. https://doi.org/10.1016/j.nucmedbio.2024.108971
86. Sartor O, de Bono J, Chi KN et al (2021) Lutetium-177–PSMA-617 for metastatic castration-resistant prostate cancer. N Engl J Med 385:1091–1103. https://doi.org/10.1056/nejmoa2107322
87. Sandhu S, Guo C, Hofman MS (2021) Radionuclide therapy in prostate cancer: from standalone to combination PSMA theranostics. J Nucl Med 62:1660–1668. https://doi.org/10.2967/jnumed.120.243295
88. Violet J, Sandhu S, Iravani A et al (2020) Long-term follow-up and outcomes of retreatment in an expanded 50-patient single-center phase II prospective trial of ^{177}Lu-PSMA-617 theranostics in metastatic castration-resistant prostate cancer. J Nucl Med 61:857–865. https://doi.org/10.2967/jnumed.119.236414
89. Rahbar K, Ahmadzadehfar H, Kratochwil C et al (2017) German multicenter study investigating 177Lu-PSMA-617 radioligand therapy in advanced prostate cancer patients. J Nucl Med 58:85–90. https://doi.org/10.2967/jnumed.116.183194
90. Fallah J, Agrawal S, Gittleman H et al (2023) FDA approval summary: Lutetium Lu 177 vipivotide tetraxetan for patients with metastatic castration-resistant prostate cancer. Clin Cancer Res 29:1651–1657. https://doi.org/10.1158/1078-0432.CCR-22-2875

91. Ahmadzadehfar H, Seifert R, Afshar-Oromieh A et al (2024) Prostate cancer theranostics with 177Lu-PSMA. Semin Nucl Med 54:581–590
92. Brandt M, Cardinale J, Aulsebrook ML et al (2018) An overview of PET radiochemistry, part 2: Radiometals. J Nucl Med 59:1500–1506
93. Evans BJ, King AT, Katsifis A et al (2020) Methods to enhance the metabolic stability of peptide-based PET radiopharmaceuticals. Molecules. https://doi.org/10.3390/molecules25102314
94. Benešová M, Bauder-Wüst U, Schäfer M et al (2016) Linker modification strategies to control the prostate-specific membrane antigen (PSMA)-targeting and pharmacokinetic properties of DOTA-conjugated PSMA inhibitors. J Med Chem 59:1761–1775. https://doi.org/10.1021/acs.jmedchem.5b01210
95. Liu T, Nedrow-Byers JR, Hopkins MR, Berkman CE (2011) Spacer length effects on in vitro imaging and surface accessibility of fluorescent inhibitors of prostate specific membrane antigen. Bioorg Med Chem Lett 21:7013–7016. https://doi.org/10.1016/j.bmcl.2011.09.115
96. Silva F, Cabral Campello MP, Paulo A (2021) materials radiolabeled gold nanoparticles for imaging and therapy of cancer. Materials. https://doi.org/10.3390/ma14010004
97. Sakore P, Bhattacharya S, Belemkar S et al (2024) The theranostic potential of green nanotechnology-enabled gold nanoparticles in cancer: a paradigm shift on diagnosis and treatment approaches. Results Chem. https://doi.org/10.1016/j.rechem.2023.101264
98. Dziawer Ł, Majkowska-Pilip A, Gaweł D et al (2019) Trastuzumab-modified gold nanoparticles labeled with 211 At as a prospective tool for local treatment of HER2-positive breast cancer. Nanomaterials. https://doi.org/10.3390/nano9040632
99. Rasaneh S, Rajabi Hossein H, Hossein Babaei M, Johari Daha F (2010) Toxicity of trastuzumab labeled 177Lu on MCF7 and SKBr 3 cell lines. Appl Radiat Isot 68:1964–1966. https://doi.org/10.1016/j.apradiso.2010.05.004
100. Yang W, Xia B, Wang L et al (2021) Shape effects of gold nanoparticles in photothermal cancer therapy. Mater Today Sustain. https://doi.org/10.1016/j.mtsust.2021.100078
101. Xu X, Chong Y, Liu X et al (2019) Multifunctional nanotheranostic gold nanocages for photoacoustic imaging guided radio/photodynamic/photothermal synergistic therapy. Acta Biomater 84:328–338. https://doi.org/10.1016/j.actbio.2018.11.043
102. Juliyanto S, Dita Pertiwi L, Nurmanjaya A et al (2024) Phytosynthesis of gold-198 nanoparticles for a potential therapeutic radio-photothermal agent. Appl Radiat Isot. https://doi.org/10.1016/j.apradiso.2023.111141
103. Tiwari S, Verma SK, Bhagat P et al (2021) An overview of the phytosynthesis of various metal nanoparticles. 3 Biotech. https://doi.org/10.1007/s13205-021-03014-0
104. Thatyana M, Dube NP, Kemboi D et al (2023) Advances in phytonanotechnology: a plant-mediated green synthesis of metal nanoparticles using Phyllanthus plant extracts and their antimicrobial and anticancer applications. Nanomaterials. https://doi.org/10.3390/nano13192616
105. Ahmad T, Iqbal J, Bustam MA et al (2021) A critical review on phytosynthesis of gold nanoparticles: issues, challenges and future perspectives. J Clean Prod. https://doi.org/10.1016/j.jclepro.2021.127460
106. Muniyappan N, Pandeeswaran M, Amalraj A (2021) Green synthesis of gold nanoparticles using *Curcuma pseudomontana* isolated curcumin: its characterization, antimicrobial, antioxidant and anti- inflammatory activities. Environ Chem Ecotoxicol 3:117–124. https://doi.org/10.1016/j.enceco.2021.01.002
107. Hani U, Rahamathulla M, Osmani RA et al (2020) Recent advances in novel drug delivery systems and approaches for management of breast cancer: a comprehensive review. J Drug Deliv Sci Technol. https://doi.org/10.1016/j.jddst.2020.101505
108. Zeinali M, Abbaspour-Ravasjani S, Ghorbani M et al (2020) Nanovehicles for co-delivery of anticancer agents. Drug Discov Today 25:1416–1430
109. Ali S, Iqbal M, Naseer A et al (2021) State of the art of gold (Au) nanoparticles synthesis via green routes and applications: a review. Environ Nanotechnol Monit Manag. https://doi.org/10.1016/j.enmm.2021.100511
110. Jannathul Firdhouse M, Lalitha P (2022) Biogenic green synthesis of gold nanoparticles and their applications – A review of promising properties. Inorg Chem Commun 143:109800
111. Abd El-Moaty HI, Soliman NA, Hamad RS et al (2021) Comparative therapeutic effects of *Pituranthos tortuosus* aqueous extract and phyto-synthesized gold nanoparticles on *Helicobacter pylori*, diabetic and cancer proliferation. S Afr J Bot 139:167–174. https://doi.org/10.1016/j.sajb.2021.02.009
112. Goswami S, Pant HJ, Biswal J et al (2016) Synthesis, characterization and application of Au-198 nanoparticles as radiotracer for industrial applications. Appl Radiat Isot 111:18–25. https://doi.org/10.1016/j.apradiso.2016.01.028
113. Silva F, Zambre A, Campello MPC et al (2016) Interrogating the role of receptor-mediated mechanisms: biological fate of peptide-functionalized radiolabeled gold nanoparticles in tumor mice. Bioconjug Chem 27:1153–1164. https://doi.org/10.1021/acs.bioconjchem.6b00102
114. Reznickova A, Slavikova N, Kolska Z et al (2019) PEGylated gold nanoparticles: stability, cytotoxicity and antibacterial activity. Colloids Surf A Physicochem Eng Asp 560:26–34. https://doi.org/10.1016/j.colsurfa.2018.09.083
115. Zhang J, Mou L, Jiang X (2020) Surface chemistry of gold nanoparticles for health-related applications. Chem Sci 11:923–936
116. Pellico J, Gawne PJ, T. M. De Rosales R (2021) Radiolabelling of nanomaterials for medical imaging and therapy. Chem Soc Rev 50:3355–3423
117. Coenen HH, Gee AD, Adam M et al (2017) Consensus nomenclature rules for radiopharmaceutical chemistry: setting the record straight. Nucl Med Biol 55:v–xi
118. Morales-Avila E, Ferro-Flores G, Ocampo-García BE et al (2011) Multimeric system of 99mTc-labeled gold nanoparticles conjugated to c[RGDfK(C)] for molecular imaging of tumor α(v) β(3) expression. Bioconjug Chem 22:913–922. https://doi.org/10.1021/bc100551s
119. Ocampo-García BE, Ramírez FdeM, Ferro-Flores G et al (2011) 99mTc-labelled gold nanoparticles capped with HYNIC-peptide/mannose for sentinel lymph node detection. Nucl Med Biol 38(1):1–11. https://doi.org/10.1016/j.nucmedbio.2010.07.007
120. Vilchis-Juárez A, Ferro-Flores G, Santos-Cuevas C et al (2014) Molecular targeting radiotherapy with cyclo-RGDfK(C) peptides conjugated to ^{177}Lu-labeled gold nanoparticles in tumor-bearing mice. J Biomed Nanotechnol 10:393–404. https://doi.org/10.1166/jbn.2014.1721
121. Luna-Gutiérrez M, Ferro-Flores G, Ocampo-García B et al (2012) ^{177}Lu-labeled monomeric, dimeric and multimeric RGD peptides for the therapy of tumors expressing α(ν)β(3) integrins. J Labelled Comp Radiopharm 55:140–148. https://doi.org/10.1002/jlcr.2910
122. Yook S, Cai Z, Lu Y et al (2016) Intratumorally injected 177lu-labeled gold nanoparticles: gold nanoseed brachytherapy with application for neoadjuvant treatment of locally advanced breast cancer. J Nucl Med. https://doi.org/10.2967/jnumed.115.168906
123. Cai Z, Yook S, Lu Y et al (2017) Local radiation treatment of HER2-positive breast cancer using trastuzumab-modified gold nanoparticles labeled with 177Lu. Pharm Res 34:579–590. https://doi.org/10.1007/s11095-016-2082-2

124. Shabbir R, Mingarelli M, Cabello G et al (2021) EGFR targeting of [177Lu] gold nanoparticles to colorectal and breast tumour cells: affinity, duration of binding and growth inhibition of Cetuximab-resistant cells. J King Saud Univ. https://doi.org/10.1016/j.jksus.2021.101573
125. Mittal S, Sharma R, Sarma HD, Mallia MB (2022) Hypoxia targeting lutetium-177-labeled nitroimidazole-decorated gold particles as cancer theranostic nanoplatforms. Mater Adv 3:1993–1999. https://doi.org/10.1039/d1ma01123e
126. Georgiou CJ, Cai Z, Alsaden N et al (2023) Treatment of orthotopic U251 human glioblastoma multiforme tumors in NRG mice by convection-enhanced delivery of gold nanoparticles labeled with the β-particle-emitting radionuclide, 177Lu. Mol Pharm 20:582–592. https://doi.org/10.1021/acs.molpharmaceut.2c00815
127. Salvanou EA, Stellas D, Tsoukalas C et al (2020) A proof-of-concept study on the therapeutic potential of au nanoparticles radiolabeled with the alpha-emitter actinium-225. Pharmaceutics. https://doi.org/10.3390/pharmaceutics12020188
128. Chilug EL, Ciucă MD, Lavric V et al (2021) Gold nanoparticles-based radiopharmaceuticals for nuclear molecular imaging and therapy applications. UPB Sci Bulletin, Ser B: Chem Mater Sci 83:73–90
129. Yook S, Lu Y, Jeong JJ et al (2016) Stability and biodistribution of thiol-functionalized and ^{177}Lu-labeled metal chelating polymers bound to gold nanoparticles. Biomacromol 17:1292–1302. https://doi.org/10.1021/acs.biomac.5b01642
130. Luna-Gutiérrez M, Ferro-Flores G, Ocampo-García BE et al (2013) A Therapeutic System of 177 Lu-labeled Gold Nanoparticles-RGD Internalized in Breast Cancer Cells Article. J Mex Chem Soc 57:212–219
131. Kang JS, Taton TA (2012) Oligothiol graft-copolymer coatings stabilize gold nanoparticles against harsh experimental conditions. Langmuir 28:16751–16760. https://doi.org/10.1021/la301249a
132. Zopes D, Stein B, Mathur S, Graf C (2013) Improved stability of "naked" gold nanoparticles enabled by in situ coating with mono and multivalent thiol PEG ligands. Langmuir 29:11217–11226. https://doi.org/10.1021/la4012058
133. Zajac A, Song D, Qian W, Zhukov T (2007) Protein microarrays and quantum dot probes for early cancer detection. Colloids Surf B Biointerfaces 58:309–314. https://doi.org/10.1016/j.colsurfb.2007.02.019
134. Mangadlao JD, Wang X, McCleese C et al (2018) Prostate-Specific Membrane Antigen Targeted Gold Nanoparticles for Theranostics of Prostate Cancer. ACS Nano 12:3714–3725. https://doi.org/10.1021/acsnano.8b00940
135. Luo D, Wang X, Zeng S et al (2019) Prostate-specific membrane antigen targeted gold nanoparticles for prostate cancer radiotherapy: does size matter for targeted particles? Chem Sci 10:8119–8128. https://doi.org/10.1039/c9sc02290b
136. Wang J, Li L, Li Y et al (2023) PSMA1-mediated ultrasmall gold nanoparticles facilitate tumor targeting and MR/CT/NIRF multimodal detection of early-stage prostate cancer. Nanomedicine. https://doi.org/10.1016/j.nano.2022.102617
137. Subiel A, Ashmore R, Schettino G (2016) Standards and methodologies for characterizing radiobiological impact of high-Z nanoparticles. Theranostics 6:1651–1671
138. Huang P, Bao L, Zhang C et al (2011) Folic acid-conjugated silica-modified gold nanorods for X-ray/CT imaging-guided dual-mode radiation and photo-thermal therapy. Biomaterials 32:9796–9809. https://doi.org/10.1016/j.biomaterials.2011.08.086
139. Neshastehriz A, Tabei M, Maleki S et al (2017) Photothermal therapy using folate conjugated gold nanoparticles enhances the effects of 6 MV x-ray on mouth epidermal carcinoma cells. J Photochem Photobiol B 172:52–60. https://doi.org/10.1016/j.jphotobiol.2017.05.012
140. Liu Y, Liu X, Jin X et al (2015) The dependence of radiation enhancement effect on the concentration of gold nanoparticles exposed to low- and high-LET radiations. Phys Med 31:210–218. https://doi.org/10.1016/j.ejmp.2015.01.006
141. Scheffer A, Engelhard C, Sperling M, Buscher W (2008) ICP-MS as a new tool for the determination of gold nanoparticles in bioanalytical applications. Anal Bioanal Chem 390:249–252. https://doi.org/10.1007/s00216-007-1576-5
142. Sicard-Roselli C, Brun E, Gilles M et al (2014) A new mechanism for hydroxyl radical production in irradiated nanoparticle solutions. Small 10:3338–3346. https://doi.org/10.1002/smll.201400110
143. Woolley JF, Stanicka J, Cotter TG (2013) Recent advances in reactive oxygen species measurement in biological systems. Trends Biochem Sci 38:556–565
144. Ngwa W, Korideck H, Kassis AI et al (2013) In vitro radiosensitization by gold nanoparticles during continuous low-dose-rate gamma irradiation with I-125 brachytherapy seeds. Nanomedicine 9:25–27. https://doi.org/10.1016/j.nano.2012.09.001
145. Miladi I, Alric C, Dufort S et al (2014) The in vivo radiosensitizing effect of gold nanoparticles based mri contrast agents. Small 10:1116–1124. https://doi.org/10.1002/smll.201302303
146. Zheng Y, Hunting DJ, Ayotte P, Sanche L (2008) Radiosensitization of DNA by gold nanoparticles irradiated with high-energy electrons. Radiat Res 169:19–27. https://doi.org/10.1667/RR1080.1
147. Gupta N, Malviya R (2021) Understanding and advancement in gold nanoparticle targeted photothermal therapy of cancer. Biochimica et Biophysica Acta (BBA). https://doi.org/10.1016/j.bbcan.2021.188532
148. Yue K, Nan J, Zhang X et al (2016) Photothermal effects of gold nanoparticles induced by light emitting diodes. Appl Therm Eng 99:1093–1100. https://doi.org/10.1016/j.applthermaleng.2016.01.077
149. Iqbal S, Fakhar-e-Alam M, Alimgeer KS et al (2021) Mathematical modeling and experimental analysis of the efficacy of photodynamic therapy in conjunction with photo thermal therapy and PEG-coated Au-doped TiO2 nanostructures to target MCF-7 cancerous cells. Saudi J Biol Sci 28:1226–1232. https://doi.org/10.1016/j.sjbs.2020.11.086
150. Guo Z, Xin Y, Yang L et al (2022) Biomimetic nanotherapeutics based on oxygen supply and ultrasmall Cu-Se-Au alloy nanoparticles for boosting radio-photothermal ablation of breast cancer. Nano Today. https://doi.org/10.1016/j.nantod.2022.101587
151. Shi X, Li Q, Zhang C et al (2021) Semiconducting polymer nano-radiopharmaceutical for combined radio-photothermal therapy of pancreatic tumor. J Nanobiotechnology. https://doi.org/10.1186/s12951-021-01083-0
152. Fikri A, Pertiwi LD, Forentin AM et al (2024) Phytosynthesis of [198Au]Au@SiO2 core–shell nanoparticles for potential radio-photothermal therapy. J Radioanal Nucl Chem 333:3807–3817. https://doi.org/10.1007/s10967-024-09549-9
153. Zhou M, Chen Y, Adachi M et al (2015) Single agent nanoparticle for radiotherapy and radio-photothermal therapy in anaplastic thyroid cancer. Biomaterials 57:41–49. https://doi.org/10.1016/j.biomaterials.2015.04.013
154. Chen L, Zhong X, Yi X et al (2015) Radionuclide ^{131}I labeled reduced graphene oxide for nuclear imaging guided combined radio- and photothermal therapy of cancer. Biomaterials 66:21–28. https://doi.org/10.1016/j.biomaterials.2015.06.043